JAMES | Journal of Advances in Modeling Earth Systems

RESEARCH ARTICLE
10.1029/2019MS001882

Special Section:
Community Earth System Model version 2 (CESM2) Special Collection

The Chemistry Mechanism in the Community Earth System Model Version 2 (CESM2)

Louisa K. Emmons[1], Rebecca H. Schwantes[1,2,3], John J. Orlando[1], Geoff Tyndall[1], Douglas Kinnison[1], Jean-François Lamarque[1], Daniel Marsh[1], Michael J. Mills[1], Simone Tilmes[1], Charles Bardeen[1], Rebecca R. Buchholz[1], Andrew Conley[1], Andrew Gettelman[1], Rolando Garcia[1], Isobel Simpson[4], Donald R. Blake[4], Simone Meinardi[4], and Gabrielle Pétron[5]

[1]National Center for Atmospheric Research, Boulder, CO, USA, [2]Now at Cooperative Institute for Research in Environmental Sciences, University of Colorado, Boulder, CO, USA, [3]Now at Chemical Sciences Laboratory, National Oceanic and Atmospheric Administration, Boulder, CO, USA, [4]Department of Chemistry, University of California, Irvine, CA, USA, [5]NOAA Earth System Research Laboratory, Boulder, CO, USA

Key Points:
- This paper fully documents the significant updates to the chemistry mechanisms in version 2 of the Community Earth System Model
- The new tropospheric chemistry scheme improves representation of isoprene oxidation as well as other ozone precursors over earlier versions
- The simulation of tropospheric ozone is improved in comparison to observations

Supporting Information:
- Supporting Information S1
- Table S1
- Table S2

Correspondence to:
L. K. Emmons,
emmons@ucar.edu

Citation:
Emmons, L. K., Schwantes, R. H., Orlando, J. J., Tyndall, G., Kinnison, D., Lamarque, J.-F., et al. (2020). The Chemistry Mechanism in the Community Earth System Model version 2 (CESM2). *Journal of Advances in Modeling Earth Systems*, *12*, e2019MS001882. https://doi.org/10.1029/2019MS001882

Received 27 AUG 2019
Accepted 17 MAR 2020
Accepted article online 24 MAR 2020

Abstract The Community Earth System Model version 2 (CESM2) includes a detailed representation of chemistry throughout the atmosphere in the Community Atmosphere Model with chemistry and Whole Atmosphere Community Climate Model configurations. These model configurations use the Model for Ozone and Related chemical Tracers (MOZART) family of chemical mechanisms, covering the troposphere, stratosphere, mesosphere, and lower thermosphere. The new MOZART tropospheric chemistry scheme (T1) has a number of updates over the previous version (MOZART-4) in CESM, including improvements to the oxidation of isoprene and terpenes, organic nitrate speciation, and aromatic speciation and oxidation and thus improved representation of ozone and secondary organic aerosol precursors. An evaluation of the present-day simulations of CESM2 being provided for Climate Model Intercomparison Project round 6 (CMIP6) is presented. These simulations, using the anthropogenic and biomass burning emissions from the inventories specified for CMIP6, as well as online calculation of emissions of biogenic compounds, lightning NO, dust, and sea salt, indicate an underestimate of anthropogenic emissions of a variety of compounds, including carbon monoxide and hydrocarbons. The simulation of surface ozone in the southeast United States is improved over previous model versions, largely due to the improved representation of reactive nitrogen and organic nitrate compounds resulting in a lower ozone production rate than in CESM1 but still overestimates observations in summer. The simulation of tropospheric ozone agrees well with ozonesonde observations in many parts of the globe. The comparison of NO_x and PAN to aircraft observations indicates the model simulates the nitrogen budget well.

Plain Language Summary The set of chemical reactions for tropospheric chemistry used in the Community Earth System Model version 2 (CESM2) has been updated significantly over CESM1 in the Community Atmosphere Model with chemistry (CAM-chem) and Whole Atmosphere Community Climate Model (WACCM) configurations. The emissions used for the CESM2 simulations are documented here, with anthropogenic and biomass burning emissions based on the specified inventories for Climate Model Intercomparison Project 6 (CMIP6), and emissions of biogenic compounds, lightning NO, dust, and sea salt are calculated online and dependent on the simulated meteorology. Evaluation of the CAM-chem and WACCM configurations of CESM2 with observations indicate an underestimate of anthropogenic emissions of a variety of compounds, including carbon monoxide and hydrocarbons. The updated chemistry leads to an improvement in the simulation of tropospheric ozone.

1. Introduction

The chemical mechanism associated with the Model of Ozone and Related chemical Tracers (MOZART), a chemical transport model for the troposphere, has evolved significantly since its first development. The first version of MOZART had 46 transported chemical species to represent tropospheric ozone production based on nitrogen oxides (NO_x), methane (CH_4), carbon monoxide (CO), and nonmethane hydrocarbons (NMHCs), including specific C_2 and C_3 alkanes and alkenes (ethane, ethene, propane, and propene) and isoprene (C_5H_8) as well as lumped larger hydrocarbons (treated as butane) and a lumped monoterpene

(Brasseur et al., 1998). The improvements introduced in MOZART-2 included not only a number of changes to physical parameterizations and transport but also updates to the chemical mechanism (Horowitz et al., 2003). The MOZART-2 chemistry had 63 chemical species with an updated isoprene oxidation scheme over MOZART-1, which included the representation of a few lumped hydroperoxides and isoprene nitrates. Heterogeneous uptake of N_2O_5 and NO_3 on sulfate aerosols (based on a prescribed distribution) were also added in this version. The oxidation of the lumped hydrocarbons and monoterpenes remained the same as MOZART-1 and was represented with the oxidation products of smaller compounds (propane and isoprene, respectively). Versions 3 and 4 of MOZART were developed in parallel, with MOZART-3 including a detailed stratospheric chemistry mechanism added to MOZART-2 (Kinnison et al., 2007), while MOZART-4 included a further expansion of the tropospheric chemistry mechanism to 85 gas-phase species, including more specific representation of larger hydrocarbons with a lumped alkane, a lumped alkene, and a lumped aromatic species with corresponding oxidation products (Emmons et al., 2010). A summary of the species included in MOZART-1, -2 and -4, highlighting the evolution of the complexity of the tropospheric chemical mechanism, is shown in Table 1. The MOZART-3 stratospheric chemistry and MOZART-4 mechanism were combined and coupled to the Community Atmosphere Model (CAM) to create CAM-chem (Lamarque et al., 2012; Tilmes et al., 2015; Tilmes et al., 2016), a component of the Community Earth System Model (CESM). The neutral and ion chemistry of the mesosphere and lower thermosphere was included in the CAM chemistry scheme for the Whole Atmosphere Community Climate Model (WACCM) configuration, which has a model top at approximately 140 km (Marsh et al., 2007).

While the offline chemical transport model MOZART is no longer being developed, the MOZART chemical mechanism continues to be updated based on recent laboratory measurements and kinetics evaluations (e.g., Burkholder et al., 2015) and is expanded when necessary to represent more chemical species to improve the model representation of atmospheric composition. However, a balance must be found between the number of species that need to be represented and computing efficiency. The latest expansion of the MOZART tropospheric chemistry (referred to as "MOZART-T1") is motivated by improved understanding of the oxidation processes of isoprene through laboratory measurements (Wennberg et al., 2018), as well as a need to better represent precursors of secondary organic aerosols. New field measurements of an increasing number of compounds, such as isoprene oxidation products, as well as individual aromatic and terpene hydrocarbons, also allow for more precise model evaluation (Fisher et al., 2016; Travis et al., 2016).

This paper presents the details of the chemical mechanism, covering the troposphere to the lower thermosphere, available in CESM2 (Danabasoglu et al., 2020). CESM2 with chemistry can be run in two main configurations: CAM6-chem, based on version 6 of the Community Atmosphere Model (CAM6) and WACCM6 (Gettelman et al., 2019). The default WACCM6 configuration uses a chemistry mechanism that represents the troposphere, stratosphere, mesosphere, and lower thermosphere (TSMLT1). Options for running WACCM6 with middle atmosphere (MA) chemistry or specified chemistry (SC) exist to reduce computational burdens, as described in Gettelman et al. (2019), but are not discussed further here. CAM6-chem, with model top at ~45 km, is run with the tropospheric and stratospheric (TS1) chemistry. A version of the troposphere-only mechanism (T1) is used in WRF-Chem V.4.0 and higher, where it is coupled to the GOCART aerosol scheme (MOZCART). The complete list of compounds for all of the CESM2 MOZART chemistry schemes is given in Table S1 in the supporting information, and the chemical mechanism for T1, TS1 (CAM-chem), and TSMLT1 (WACCM) configurations is listed in Table S2.

CESM2 has been run with chemistry in several configurations for the Coupled Model Intercomparison Project round 6 (CMIP6) (Eyring et al., 2016) and other applications. All simulations shown here are run at the standard 0.9° × 1.25° (latitude by longitude) horizontal resolution. Both WACCM6 and CAM6-chem have been run in free-running configurations, with specified sea surface temperatures and thermodynamic sea ice (referred to as "AMIP," for 1950–2014) (Danabasoglu, 2019a) or with fully coupled ocean and sea ice models ("HIST," from 1850 to 2014) (Danabasoglu, 2019b). Both WACCM6 and CAM6-chem are coupled to the interactive Community Land Model (CLM5), which provides biogenic emissions and handles dry deposition. Simulations of CAM6-chem and WACCM6 have also been performed with nudging to reanalysis meteorology fields, labeled Specified Dynamics (SD). The SD simulations presented here used a 50-hr Newtonian relaxation time to Modern-Era Retrospective analysis for Research and Applications (MERRA2) fields of temperature, horizontal winds, and surface fluxes (Molod et al., 2015).

Table 1
Comparison of Species in MOZART Tropospheric Chemical Mechanisms

MOZART-1	MOZART-2	MOZART-4	MOZART-T1
46 gas-phase species 28 photolysis, 112 kinetic reactions	63 gas-phase species 32 photolysis, 135 kinetic reactions	85 gas-phase species 39 photolysis, 157 kinetic reactions	151 gas-phase species 65 photolysis, 287 kinetic reactions
O_x(=O1D + O3P + O_3), H2, OH, HO2, H2O2, NO_x(=N + NO + NO_2), NO3, HNO3, HO2NO2, N2O5, N2O	OX, H2, OH, HO2, H2O2, N, NO, NO2, NO3, HNO3, HO2NO2, N2O5, N2O	O3, O1D, O, H2, OH, HO2, H2O2, NO, NO2, NO3, HNO3, HO2NO2, N2O5, N2O	O3, O1D, O, H2, OH, HO2, H2O2, NO, NO2, NO3, HNO3, HO2NO2, N2O5, N2O
CO, CH4, CH3O2, CH3OOH, CH2O	CO, CH4, CH3O2, CH3OOH, CH2O, **CH3OH**	CO, CH4, CH3O2, CH3OOH, CH2O, CH3OH, **HCOOH**, **HOCH2OO**	CO, CH4, CH3O2, CH3OOH, CH2O, CH3OH, HCOOH, HOCH2OO
C2H6, C2H5O2, C2H5OOH, C2H4, GLYALD, CH3CHO, CH3CO3, CH3COOOH	C2H6, C2H5O2, C2H5OOH, C2H4, **EO**, **EO2**, GLYALD, CH3CHO, CH3CO3, CH3COOOH, **C2H5OH**	C2H6, C2H5O2, C2H5OOH, C2H4, EO, EO2, GLYALD, CH3CHO, CH3CO3, CH3COOOH, C2H5OH, **CH3COOH**, **C2H2, GLYOXAL**	C2H6, C2H5O2, C2H5OOH, C2H4, EO, EO2, GLYALD, CH3CHO, CH3CO3, CH3COOOH, C2H5OH, CH3COOH, C2H2, GLYOXAL
C3H8, C3H6, C3H7O2, PO2, C3H7OOH, POOH, CH3COCH3, RO2, ROOH, HYAC, CH3COCHO	C3H8, C3H6, C3H7O2, PO2, C3H7OOH, POOH, CH3COCH3, RO2, ROOH, HYAC, CH3COCHO	C3H8, C3H6, C3H7O2, PO2, C3H7OOH, POOH, CH3COCH3, RO2, ROOH, HYAC, CH3COCHO	C3H8, C3H6, C3H7O2, PO2, C3H7OOH, POOH, CH3COCH3, RO2, ROOH, HYAC, CH3COCHO
PAN, MPAN, ONIT	PAN, MPAN, ONIT, **ONITR**	PAN, MPAN, ONIT, ONITR	PAN, MPAN, ONIT, ONITR, **ALKNIT**, **NOA**, **HONITR, ISOPNITA, ISOPNITB, PBZNIT, TERPNIT**
C4H10	C4H10	**BIGALK, ALKO2, ALKOOH, BIGENE, ENEO2, MEK, MEKO2, MEKOOH**	BIGALK, ALKO2, ALKOOH, BIGENE, ENEO2, MEK, MEKO2, MEKOOH
ISO, ISO1, MVK, MACR, MACRO2, MCO3, HYDRALD	ISOP, ISOPO2, **ISOPOOH**, MVK, MACR, MACRO2, **MACROOH**, MCO3, HYDRALD, **ISOPNO3**, **XO2**, **XOOH**	ISOP, ISOPO2, ISOPOOH, MVK, MACR, MACRO2, MACROOH, MCO3, HYDRALD, ISOPNO3, XO2, XOOH	ISOP, **ISOPAO2, ISOPBO2,** ISOPOOH, MVK, MACR, MACRO2, MACROOH, MCO3, HYDRALD, ISOPNO3, XO2, XOOH, **IEPOX, HPALD, ISOPNOOH, NC4CHO, NC4CH2OH, IVOC, SVOC**
		TOLUENE, CRESOL, TOLO2, TOLOOH, XOH, BIGALD	TOLUENE, CRESOL, TOLO2, TOLOOH, XOH, BIGALD, **BENZENE**, **XYLENES**, **BENZO2, BZOO, BENZOOH, XYLENO2, XYLENOOH, PHENOL, PHENO, PHENO2, PHENOOH, BZALD, ACBZO2, C6H5O2, C6H5OOH, BEPOMUC, TEPOMUC, BIGALD1, BIGALD2, BIGALD3, BIGALD4, XYLOL, XYLOLO2, DICARBO2, MALO2, MDIALO2**
C10H16	C10H16	C10H16, **TERPO2**, **TERPOOH**	**MTERP (*or* APIN, BPIN, MYRC, LIMON), BCARY**, TERPO2, TERPOOH, **TERPROD1, TERPROD2, TERP2O2, TERP2OOH, NTERPO2, NTERPOOH**
		SO2, DMS, NH3	SO2, DMS, NH3

Note. Mechanism species names, not chemical formulae, are listed. Bold face font indicates new species from previous version. The complete mechanisms for the earlier versions are in Brasseur et al. (1998), Horowitz et al. (2003), and Emmons et al. (2010).

CAM6-chem-SD simulations have been run for 2000 through 2018 (Buchholz et al., 2019). WACCM6-SD simulations were run for 1979–2014 and use the same emissions as the standard CMIP6 simulations. Table 2 gives a summary of the simulations used in this work.

The following sections (2 and 3) describe the updates to the tropospheric chemistry mechanisms as well as other chemical processes. A comparison of simulations using the MOZART-T1 and MOZART-4 mechanisms is presented in section 4, showing the impact of the mechanism on ozone, its precursors, and ozone production rates. Section 5 gives a summary of the emissions used for CESM2 CMIP6 simulations and released with CESM2, along with an evaluation of CAM6-chem and WACCM6 simulations with a variety of observations. The final section provides some discussion and conclusions.

Table 2
Summary of Simulations Presented

Label	CESM configuration	Meteorology	Simulation years
WACCM-HIST	CESM2 (WACCM6), fully coupled	Free-running	1850–2014
WACCM-AMIP	CESM2 (WACCM6), observed SST	Free-running	1950–2014
WACCM-SD	CESM2 (WACCM6), specified dynamics	Nudged to MERRA2	1980–2014
CAMchem-SD	CESM2 (CAM6-chem), specified dynamics	Nudged to MERRA2	2000–2018
MOZART-T1	CESM2 (CAM6-chem), specified dynamics	Nudged to MERRA2	2013
MOZART-T0	CESM2 (CAM6-chem) with MOZART-4 gas-phase chemistry	Nudged to MERRA2	2013

2. Tropospheric Chemistry Mechanism Updates

The updates to the MOZART tropospheric mechanism include an expansion of the isoprene oxidation scheme, splitting lumped aromatics and terpenes into individual species and improving their oxidation scheme, oxidation of the biogenic compound MBO, and a more detailed representation of organic nitrates. Preliminary versions of this mechanism were used in Knote et al. (2014) and He et al. (2015).

2.1. Updated Isoprene Oxidation

The chemical mechanism for isoprene oxidation in MOZART-4 included intermediate products methacrolein (MACR), methylvinyl ketone (MVK), and lumped isoprene nitrates (ONITR), along with multiple generations of peroxy radicals, with a goal of representing formaldehyde and ozone production. Recent laboratory chamber studies and theoretical calculations have provided greater details of the isoprene oxidation pathways (e.g., Paulot, Crounse, Kjaergaard, Kurten et al., 2009; Paulot, Crounse, Kjaergaard, Kroll et al., 2009; Peeters et al., 2009; Peeters et al., 2014; Wennberg et al., 2018). In addition, measurements of a number of intermediate products of isoprene oxidation have been made during field campaigns, such as the Southeast Oxidants and Aerosol Study (Carlton et al., 2018) and SEAC^{4}RS (Toon et al., 2016). The MOZART mechanism has been updated to include some of these compounds, allowing for a more thorough evaluation of the representation of chemistry in the model and improving the simulation of ozone production.

The MOZART-T1 mechanism includes two "lumped" peroxy radicals (representing the beta and delta isomers) from the reaction of isoprene with OH and one peroxy radical from reaction of isoprene with NO_3, with subsequent parameterized peroxy radical isomerization. The formation and oxidation of methyl-vinyl ketone (MVK) and methacrolein (MACR) is slightly updated from MOZART-4, with first generation hydroxyacetone (HYAC), methylglyoxal (CH3COCHO), glyoxal, and glycoaldehyde (GLYALD) formation. The reactions of peroxy radicals have been updated (Orlando & Tyndall, 2012). "Lumped" isoprene nitrate formation and chemistry has been updated. One "lumped" ISOPOOH is formed but with multiple product channels to account for partial IEPOX formation. Destruction of IEPOX is accounted for, although in a manner that is not connected to secondary organic aerosol (SOA) formation. The hydroperoxyl aldehyde isomers formed in the isomerization of the isoprene peroxy radicals are treated as single species (HPALD) in T1, with chemical losses by photolysis and reaction with OH. See Tables S1 and S2 for details.

2.2. Speciated Aromatics

The original lumped aromatic in MOZART-4 (called "TOLUENE") has been replaced by the species BENZENE, TOLUENE, and XYLENES (lumped isomers of xylene, as well as other alkyl-substituted aromatics). The representation of these separate species allows accounting for their very different lifetimes (from reaction with OH), as well as their different oxidation products, as described in Knote et al. (2014). Separate aromatic species were introduced in CESM1.2/CAM-chem, primarily as SOA precursors with a very simplified oxidation scheme (Tilmes et al., 2015). In T1, the degradation of each aromatic species includes production of glyoxal with differing yields (Calvert et al., 2002). The oxidation scheme is based on the Leeds Master Chemical Mechanism (Bloss et al., 2005). The intermediate oxidation products include several aldehydes (benzaldehyde, as well as some lumped compounds) and dicarbonyls, as well as peroxybenzoyl nitrate (PBZNIT), a compound similar to peroxy acetyl nitrate (PAN), but some of the multifunctional later generation products are ignored as they are assumed to be quickly lost via wet or dry deposition or aerosol uptake and thus have no further impact on the gas-phase chemistry. The MOZART-T1 aromatic oxidation scheme has been included in the GEOS-Chem chemical transport

model, version v9-02 (Porter et al., 2017) where it was shown to increase OH reactivity, as well as surface ozone mixing ratios in some regions.

2.3. Speciated Terpenes and Updated Oxidation

The MOZART-4 mechanism has a single lumped terpene species ("C10H16") with a very simple oxidation scheme and reaction rates based on alpha-pinene. In MOZART-T1, C10H16 has been split into four monoterpenes and one sesquiterpene, and the oxidation scheme has been expanded. The primary degradation rates for these new species are based on alpha-pinene (APIN), beta-pinene (BPIN), limonene (LIMON), myrcene (MYRC), and beta-caryophyllene (BCARY), but each species includes a number of similar terpenes in their emissions so as to better represent the total carbon emissions. These five species, however, create common lumped oxidation products in our mechanism (TERPROD1, etc.) for computational efficiency. For the CESM2 TS and TSMLT mechanisms, we have relumped the monoterpenes (APIN, BPIN, LIMON, and MYRC) into a new lumped species, MTERP, to reduce computing costs. For tropospheric studies targeting terpene chemistry and SOA formation, it is recommended to use the speciated monoterpene scheme (T1).

2.4. MBO

The reactions for the oxidation of the biogenic compound 2-methyl-3-buten-2-ol (MBO) and its oxidation products are available in the T1 mechanism as described in Knote et al. (2014). MBO has been observed to have strong emissions in evergreen forests in Colorado and California and may be important in other parts of the world (Bouvier-Brown et al., 2009). The oxidation products are rather different from both isoprene and the terpenes, which is another reason to include it specifically. For example, it has a high yield of acetone (CH_3COCH_3), while isoprene and terpenes do not. As the estimates of MBO biogenic emissions are very uncertain, there can be locations where excessive MBO emissions will lead to too high acetone mixing ratios (in comparison to observations), so this set of reactions is not included in the standard TS1 and TSMLT1 mechanisms in CESM2.

2.5. Updated Organic Nitrates

The MOZART-4 mechanism included only a couple of lumped organic nitrate compounds (ONIT and ONITR) created from a wide variety of precursors. This new mechanism adds a number of organic nitrate species. The oxidation of the lumped large alkane ("BIGALK," butanes, C_4H_{10}, and larger) now creates an alkyl nitrate, ALKNIT. Propene (C_3H_6) is oxidized (by NO_3) producing nitrooxyacetone (NOA). A lumped species that represents a mix of hydroxyl- and carbonyl-nitrates (HONITR) is a result of NO reaction with isoprene and MBO oxidation products, as well as from the lumped large alkene (BIGENE, representing butenes and larger). The two isoprene peroxy radicals formed from isoprene oxidation with OH create beta- and delta-hydroxynitrates, ISOPNITA, and ISOPNITB, which react with OH forming NOA and HONITR. ISOP + NO3 results in ISOPNOOH (nitroxy-hydroperoxide) and NC4CHO (nitrooxy-aldehyde), which then break down to NOA and other products. The terpene oxidation mechanism now creates a hydroxynitrate TERPNIT and a nitrooxy-hydroperoxide NTERPOOH; both react with OH and when photolyzed release NO_2. These new organic nitrates have parameterized heterogeneous uptake on aerosols, releasing HNO_3, with the uptake coefficients given in Table S2 for each compound (and discussed further in the next section). Comparisons of the MOZART-4 and MOZART-T1 organic nitrates are presented below (section 4).

2.6. Tropospheric Aerosols and Heterogeneous Uptake

Both WACCM and CAM-chem include the Modal Aerosol Model with 4 modes (MAM4), representing sulfate, primary and aged black carbon and organic matter, secondary organic aerosols, sea salt, and dust (Liu et al., 2016), as implemented in CESM1.2 (CAM5) (Tilmes et al., 2015). A bulk representation of ammonium aerosol is also included in CESM2 (Lamarque et al., 2012), primarily to account for nitrogen deposition which is passed to the land model for its biogeochemistry. Secondary organic aerosols are simulated using a Volatility Basis Set (VBS) representation described in detail in Tilmes et al. (2019), with gas-phase SOA precursors with a range of volatilities are produced from the oxidation of the aromatic species, terpenes and isoprene (shown in Table S2, where it is denoted by VBS-SOA).

Aerosol surface area density (SAD) is calculated based on the simulated MAM4 aerosol distributions of sulfate, black carbon, primary, and secondary organic aerosol (Mills et al., 2016). Tropospheric SAD is used in

the heterogeneous uptake reactions, including N_2O_5 hydrolysis, NO_2, and HO_2 uptake, as well as the heterogeneous conversion of the organic nitrates to nitric acid (see Table S2 for details).

3. Additional Chemistry Components

The chemistry for the stratosphere, mesosphere, and lower thermosphere in CESM2 is described in Gettelman et al. (2019) and the chemical reactions are included in Table S2. Many components of the chemistry model remain the same as in CESM1 (as described in Tilmes et al., 2016). The determination of photolysis rates uses a lookup table calculated from the Tropospheric Ultraviolet and Visible (TUV) radiation model (Kinnison et al., 2007). An error in the implementation of the wet deposition scheme (Neu & Prather, 2012) that caused weakly soluble species with a temperature-dependent Henry's law constant to have the much faster removal rate of nitric acid (HNO_3) has been corrected in CESM2. The compounds affected include acetone (CH_3COCH_3), hydrogen cyanide (HCN), and acetonitrile (CH_3CN); however, in CESM1 configurations, wet deposition generally was not applied to acetone, so this error did not have a strong impact on reactive chemistry.

The dry deposition parameterization is in general the same as in CESM1; however, an error was discovered in the stomatal uptake of ozone (Val Martin et al., 2014), which is corrected in CESM2, resulting in a slight increase in ozone dry deposition rates. In the original implementation, the sunlit and shaded fractions of the stomatal resistances were added in series, whereas they ought to be added in parallel. The correct formula is: $1/R_s = f_{sun}$*LAI*$(1/r_s^{sun}) + (1\text{-}f_{sun})$*LAI*$(1/r_s^{sha})$. In addition, the scaling of R_s by 0.2, that was applied to match observations in the original implementation is no longer needed.

The gas-phase chemical mechanism is not exactly balanced for nitrogen, because a few nitrogen-containing reaction products are assumed to be lost by wet or dry deposition or taken up by aerosols and then deposited, faster than they will react photochemically. Therefore, these compounds are not included further in the gas-phase chemistry but do need to be included in the nitrogen deposition budget for use by the land model for simulation of carbon-nitrogen cycling. Thus, additional tracers (NDEP and NHDEP) are included in the atmospheric chemistry mechanism to track the reactive nitrogen and ammonia wet and dry deposition to the land in place of the compounds not explicitly represented.

4. Comparison of MOZART-T1 to MOZART-4 Chemistry

To show the differences between the current chemistry in CESM2 and previous versions, such as in CESM1.2(CAM-chem) and MOZART-4, CESM2 was configured for this study to use the gas-phase chemistry of CESM1.2 (abbreviated as "T0" here) but keeping the aerosol scheme of CESM2 (i.e., MAM4 with VBS-SOA) to limit the differences in cloud-aerosol interactions and surface area density which is used for heterogeneous uptake of gas-phase compounds. Tilmes et al. (2019) presents in detail the impacts of the VBS-SOA scheme on atmospheric composition and climate in CESM2. These simulations (standard CESM2 with the T1 mechanism and the T0 version) were nudged to meteorological reanalyses (MERRA2) with a 50-hr Newtonian relaxation time, to reduce changes in the meteorology between the two simulations. The T0 and T1 simulations also use the same emissions, as the majority of the new compounds in the T1 mechanism are oxidation products. The T0 lumped terpene compound (C10H16) has emissions from all terpenes, which are distributed appropriately in the new T1 monoterpene and sesquiterpene species (see Table S5). The two simulations have identical deposition velocities and washout rates.

Figure 1 shows the difference in monthly mean surface ozone between MOZART-T1 and T0. The monthly mean differences are less than a few ppb; however, the changes on regional scales reflect an improved representation of the oxidation processes of ozone precursors. Both simulations use the corrected ozone dry deposition (mentioned above in section 3). In both seasons and hemispheres in the simulation with MOZART-T1, surface O_3 is generally reduced over land while slightly increased over the Southern Hemisphere oceans.

Ozone is slightly higher in the T1 simulation over ocean regions a short distance downwind from continents as a result of the more detailed representation of nitrogen reservoirs, such as organic nitrates, that are transported from source regions before releasing NO_x and forming ozone. The difference in the rate of gross ozone production between the T1 and T0 mechanisms more clearly shows the reduction of ozone production with

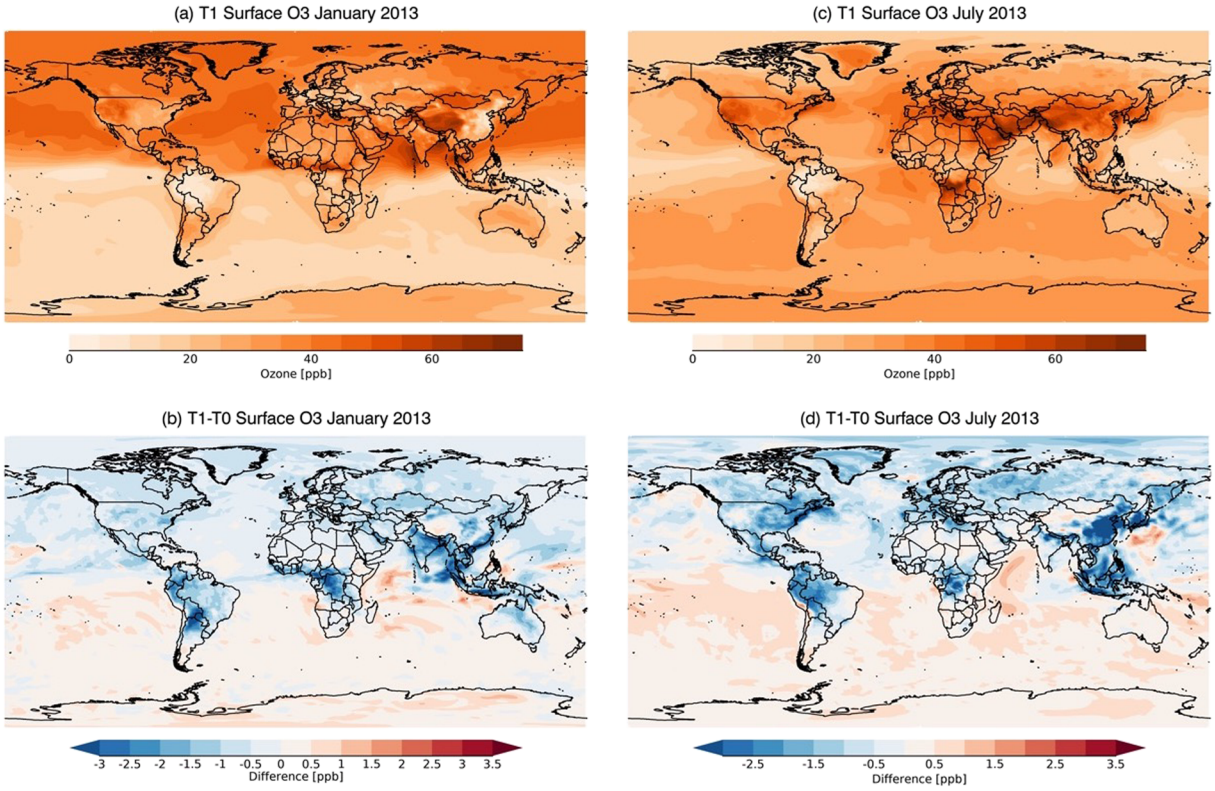

Figure 1. (a and c) Monthly mean surface ozone for January and July 2013 from MOZART-T1 and (b and d) differences between MOZART-T1 and MOZART-T0 (approximately MOZART-4).

the new T1 mechanism over land and increases over downwind ocean regions (see Figure 2). The gross ozone production rate is determined from the rate-limiting reactions, the sum of the reaction rates for NO plus HO_2 and all RO_2 species.

The global annual tropospheric ozone budget terms are quite similar for the T0 and T1 mechanisms. Table 3 shows the comparison of the tropospheric ozone burden, production and loss rates, deposition flux, and stratosphere-to-troposphere influx. The tropopause height used for this budget is the altitude at which ozone increases above 150 hPa. The ozone burden and production and loss rates for both T0 and T1 are within the interquartile range of approximately 30 models summarized in Young et al. (2018) and included in Table 3. The ozone deposition flux in both cases is below the range of the other models but only slightly.

Tropospheric OH (hydroxyl radical) is another important indicator of the impact of changes in the chemical mechanism on tropospheric chemistry. Figure 3 shows the surface OH distribution for January and July 2013 for the T1 mechanism and the difference between T0 and T1. In general, the T1 mechanism has higher OH in summer over land, for example, Australia in January and the United States and southwestern China in July. In winter over land, a slight decrease in OH is seen, with little change over the ocean in both seasons. The methane lifetime (determined from the global methane burden divided by the global annual CH_4 + OH loss rate) is slightly lower for the T1 mechanism (8.4 years for T0; 8.2 years for T1), indicating a slight increase in global tropospheric OH.

One of the most significant differences between the MOZART-T1 and MOZART-4 mechanisms is the treatment of organic nitrates. To illustrate this update, the burden of the nitrates in the T0 and T1 simulations is plotted for several regions, showing the monthly variation, in Figure 4. In the T0 mechanism, ONIT is produced from primarily anthropogenic sources while ONITR is from biogenic sources. The T1 mechanism specifies these with more detail, such as ALKNIT and NOA from primarily anthropogenic precursors alkanes and propene, while the remaining compounds shown in Figure 4 are from isoprene and terpene oxidation and therefore track the impact of biogenic sources on the reactive nitrogen budget. The updated isoprene and terpene oxidation chemistry in T1 results in slight increases in the total nitrates in summer

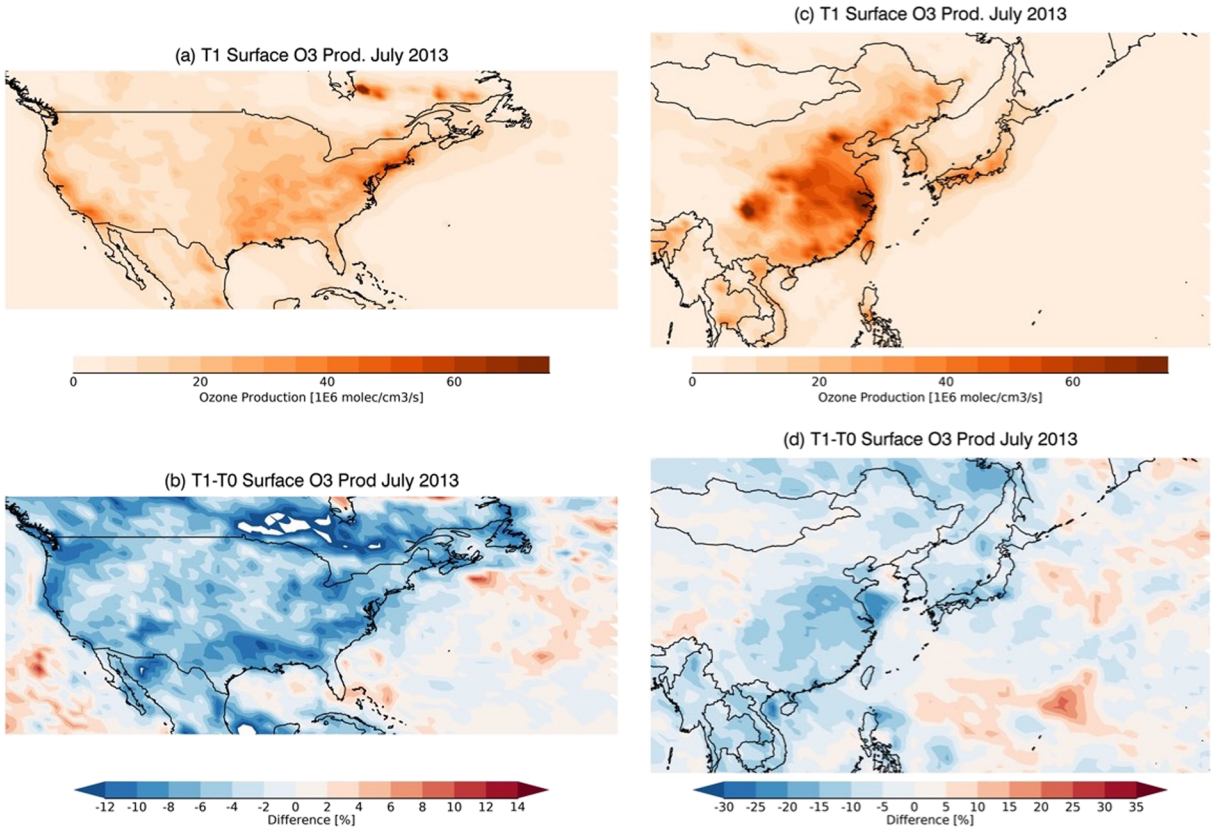

Figure 2. Ozone production rates for July 2013 from the T1 simulation over (a) United States and (c) East Asia, with differences between T1 and T0 shown in (b) and (d) (note different scales).

in SEUS and Europe and a rather large increase in Australia. In winter in SEUS, Europe and China, the T1 nitrates are slightly lower than T0, a result of a more precise representation of nitrates from primarily anthropogenic sources (e.g., alkanes). In the Amazon, where isoprene emissions dominate other sources, the T1 nitrate burden is lower than T0.

5. Results From CESM2 With Chemistry

An evaluation of the tropospheric chemistry in the simulations of CESM2 (WACCM6) for CMIP6, as well as CESM2 (CAM6-chem) as described in the introduction (see Table 2), is shown in the following sections.

5.1. Emissions for the CMIP6 Configuration of CESM2

The standard emissions released with CESM2 are based on the anthropogenic and biomass burning inventories specified for CMIP6. Anthropogenic emissions for 1750–2014 were provided from the Community Emissions Data System (CEDS) (Hoesly et al., 2017, 2018). Biomass burning emissions are described by van Marle et al. (2016, 2017) and are all emitted at the surface (without any plume-rise or specified vertical distribution of the emissions). The CMIP6 anthropogenic and biomass burning emissions are provided for a number of VOCs which must be matched to the chemical species in CESM, as listed in Table S3. Additional emissions (e.g., soil NO, oceanic CO, and hydrocarbons) are taken from the POET inventory (Granier et al., 2005). Continuous volcanic out-gassing emissions of SO_2, with 2.5% emitted as sulfate aerosols, are from the GEIA inventory (Andres & Kasgnoc, 1998). SO_2 from eruptive volcanoes is specified as well, based on the database of Volcanic Emissions for Earth System Models, version 3.11 (VolcanEESM; Neely & Schmidt, 2016).

Table 3
Tropospheric Ozone Budget, and Methane Lifetime, for T0 and T1 Simulations (for 2013), Compared to the Interquartile Range of Multiple Models from Young et al. (2018)

Budget term	T0	T1	Multimodel range
Tropospheric O_3 burden (Tg)	342	344	320–370
O_3 production rate (Tg/year)	5,078	5,134	4,500–5,200
O_3 loss rate (Tg/year)	4,489	4,498	4,000–4,800
O_3 deposition flux (Tg/year)	841	828	850–1,200
Stratospheric influx (Tg/year)	469	479	440–630

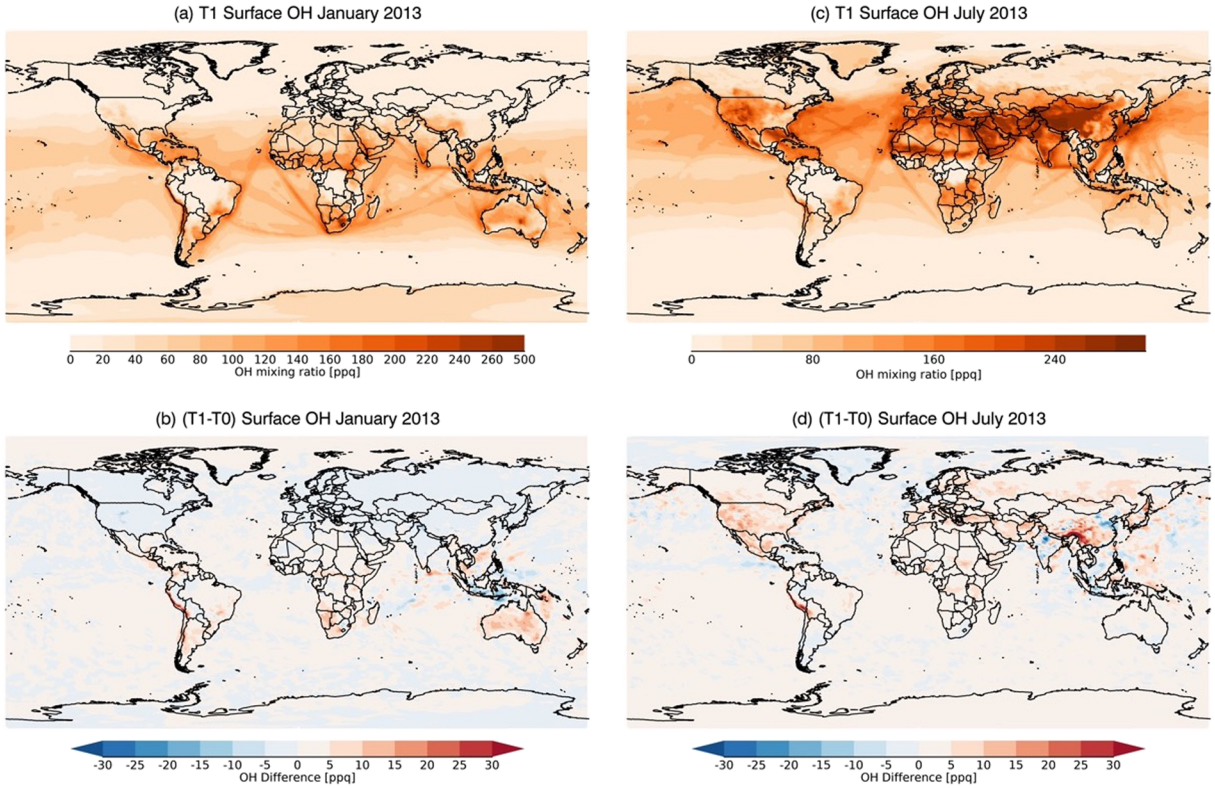

Figure 3. Surface OH mixing ratio for T1 simulations for (a) January and (b) July and differences between T1 and T0 for (c) January and (d) July.

The surface mixing ratios of greenhouse gases (methane, N_2O, and chlorofluorocarbons) are set to the fields specified for CMIP6 historical conditions and future scenarios (Meinshausen et al., 2017). The CAM6-chem simulations shown here use fire emissions from the Quick Fire Emission Dataset, which is based on observed fire detections (Darmenov & da Silva, 2015). Table S4 provides the parameters used to create the MAM4 aerosol emissions.

Biogenic emissions are calculated online using the MEGANv2.1 algorithm incorporated in the Community Land Model (CLM) (Guenther et al., 2012). The emissions of 140 compounds are available from MEGAN, and the relevant compounds are matched to the MOZART chemical species with a run-time namelist. Isoprene and a number of other compounds in MOZART have a direct match with MEGAN, while a few of the lumped MOZART species have biogenic emissions based on a combination of several MEGAN species, as listed in Table S5.

The time series (1950–2015) of emissions used to drive the WACCM-AMIP simulation are shown in Figure S1 for each species (that has emissions). The contribution of each sector is shown, including the emissions from offline files for anthropogenic and biomass burning, as well as for the biogenic emissions calculated online during the simulation. The CMIP6 emissions are available starting from 1750 and are used for the WACCM-HIST simulations but not illustrated here. The biomass burning emissions specified for CMIP6 are fairly constant with time, but the anthropogenic emissions begin increasing after 1900 with industrial development, with the majority of the increase occurring in recent decades. These plots (in Figure S1) show that the alkenes (ethene (C2H4), propene (C3H6), and lumped butenes and larger (BIGENE)) have a large relative contribution from biogenic emissions, which are often not considered in tropospheric chemistry simulations. These add approximately 35 TgC/year, which is roughly a third of the terpene emissions. Figure S2 compares the total emissions (based on diagnostic output from the simulations) for WACCM and CAM-chem cases for CMIP6 and similar configurations. Comparisons are also made to the emissions used in CAM4-chem for the Chemistry Climate Model Initiative (CCMI) (Tilmes et al., 2016). For many species (e.g., CO), the emissions are similar between CMIP6 and CCMI, but there are also large differences in NO and some VOCs. Dust and sea salt emissions are calculated online and depend on wind speed (Mahowald, Lamarque et al., 2006;

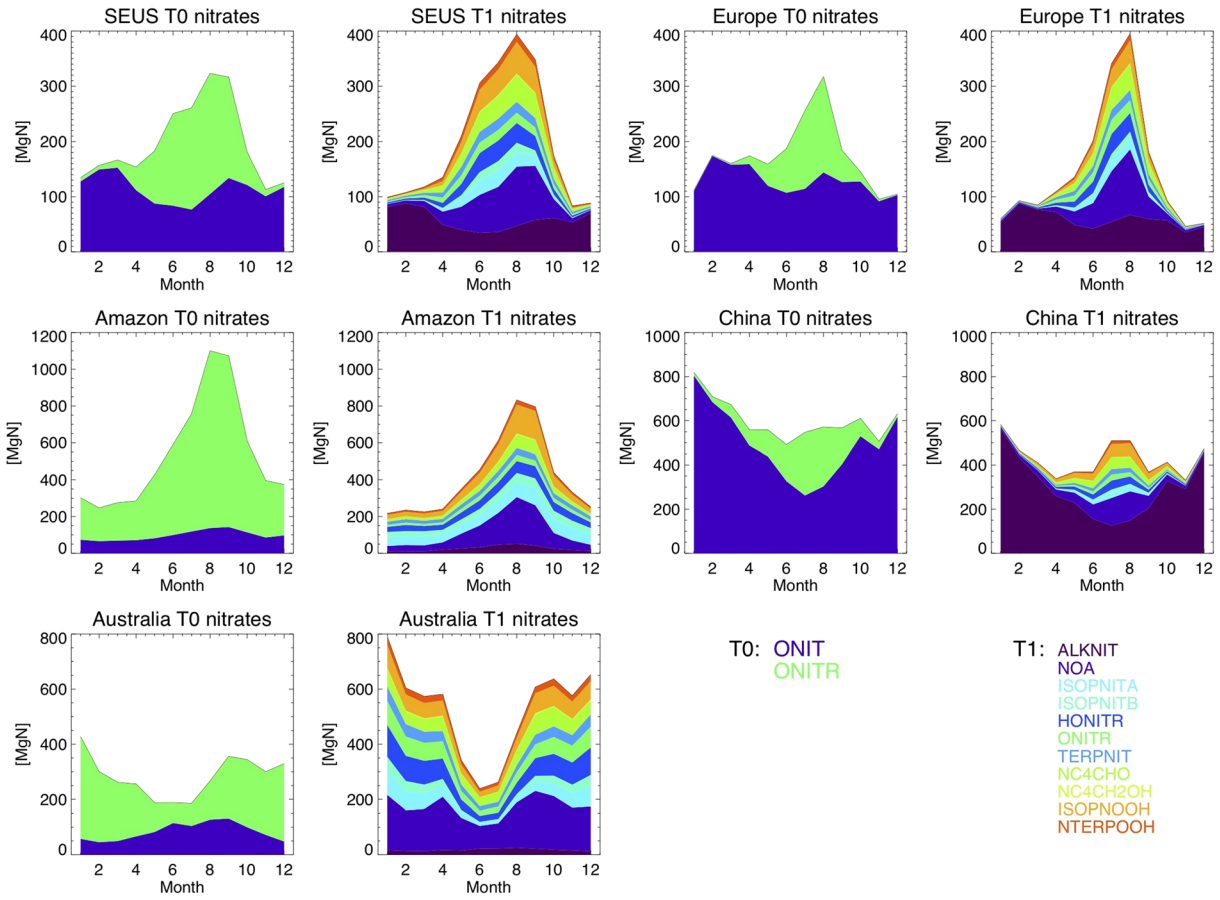

Figure 4. Organic nitrate burden (in megagrams N per year) from T0 and T1 simulations for several regions, specifically southeast United States ("SEUS," 29–40°N, 260–282°E), Europe (40–55°N, 0–30°E), the Amazon (20–0°S, 290–320°E), China (22–42°N, 102–123°E), and Australia (45–10°S, 110–155°E).

Mahowald, Muhs et al., 2006). The specified dynamics cases have systematically higher dust emissions, but lower sea salt emissions, than the free-running simulations, as shown in Figure S2. Lightning NO emissions are calculated online based on the Price et al. (1997) parameterization, as described in Lamarque et al. (2012). The emissions from the CESM2 SD simulations, as well as the CCMI simulations, are approximately 4 TgN/year, while those from the free-running WACCM6 simulations are about 3 TgN/year, with little variation over the historical period (see Figure S2). These are within the generally accepted range (3–8 TgN/year) for lightning NO emissions (Schumann & Huntrieser, 2007).

5.2. Evaluation of Tropospheric Chemistry

5.2.1. Surface Ozone Evaluation

The database of gridded surface ozone developed for the Tropospheric Ozone Assessment Report (TOAR) allows for long-term regional evaluation of modeled ozone (Schultz et al., 2017). Figure 5 shows the time series of the gridded ozone (2° × 2°) for several regions and the model mean biases for each month averaged over the region. The correlation coefficient and mean biases between each of the model simulations and the TOAR observations for the full time period, as well as for summer and winter seasons, are given in Table 4. The southeast United States shows a strong seasonal variation in the bias, with a mean bias of 13 ppb in summer (June to August), but only 2 ppb in the winter (January to March). The bias in Europe is much less (~5 ppb) though the variation in the observations is greater than in the United States. The ozone levels in Japan are higher than the other regions, and the model bias is also proportionately higher. Ozone in the Australia and New Zealand region is quite a bit lower than in the Northern Hemisphere (ranging from 15 to 35 ppb), with a small bias of ~5 ppb in summer and ~2 ppb in winter. Also shown in Table 4 are the results of the comparison of the T0 and T1 simulations presented above with the observations for 2013. For each of

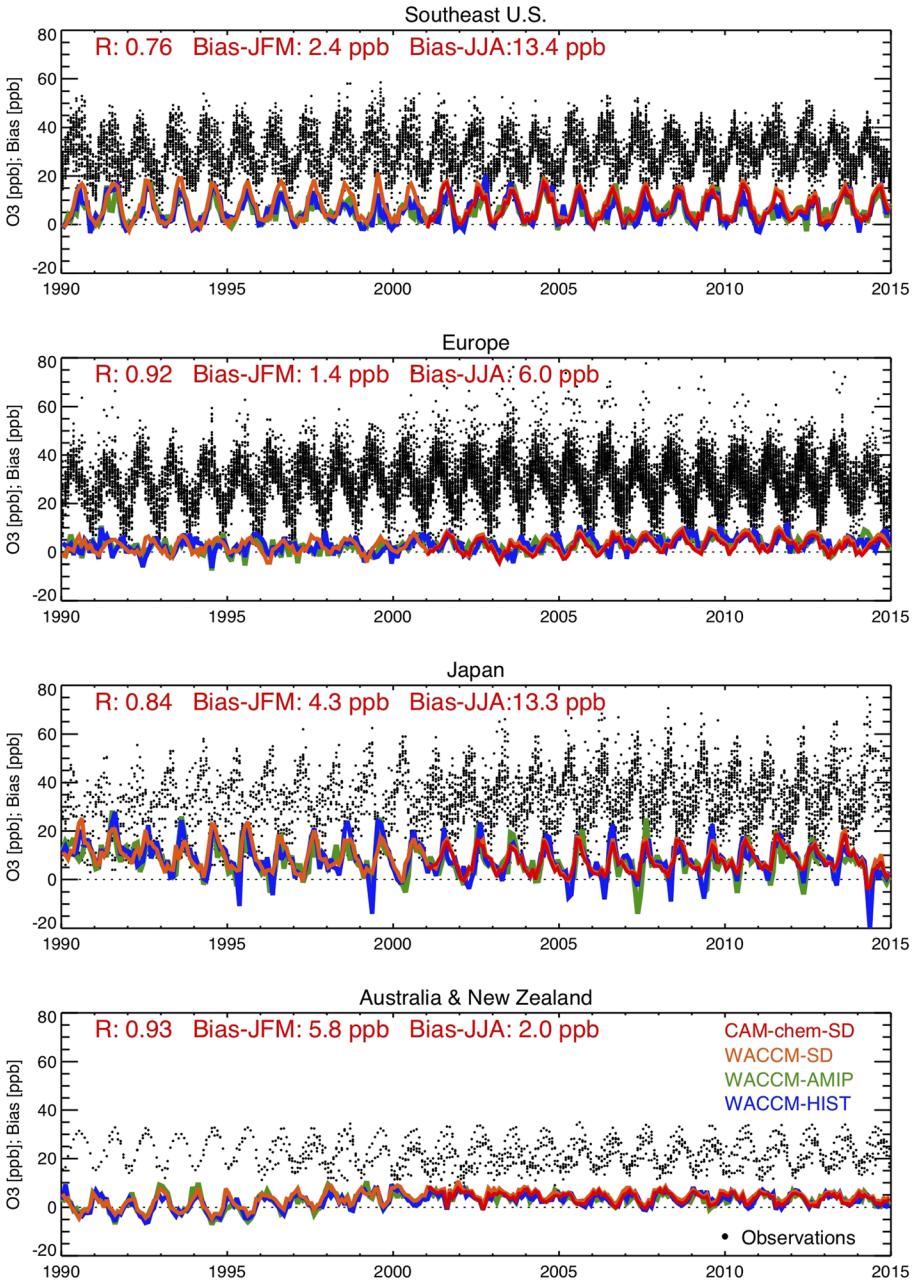

Figure 5. Observed median surface ozone from rural sites gridded at 2° × 2° from the Tropospheric Ozone Assessment Report (TOAR) data base (black points), and the regional mean biases for four CESM2 simulations (colored lines: red, CAM6-chem-SD; orange, WACCM6-SD; green, WACCM6-AMIP; and blue, WACCM6-HIST), for time series in four regions: southeast United States, Europe, Japan, and Australia–New Zealand. Pearson's correlation coefficient (*R*) and mean biases for summer and winter for CAM-chem-SD are given for each region (see Table 4 for other model statistics).

the Northern Hemisphere regions, there is a decrease in the ozone bias in T1 versus T0 in both summer (~2 ppb) and winter (~1 ppb).

5.2.2. Free Troposphere Ozone Evaluation

Here, we show several CESM2 configurations compared to the ozonesonde-based climatology compiled by Tilmes et al. (2012). Ozonesondes have been routinely launched at numerous locations for the past several decades and provide a valuable record of the evolution of ozone mixing ratios in the troposphere and stratosphere over that time. Figure 6 shows the comparison of the CESM2 simulations to the ozonesonde climatology (for 1995–2010) in Taylor-like diagrams (Taylor, 2001; Tilmes et al., 2012) at 900, 500, and 250 hPa pressure

Table 4
Statistics for Comparison of Model Simulations to Gridded Surface Ozone From the TOAR Database

Region	Model	R	Annual bias	JFM bias	JJA bias
Southeast United States	CAM-chem-SD	0.76	6.9	2.4	13.4
	WACCM-SD	0.80	8.0	2.9	15.1
	WACCM-AMIP	0.81	6.3	3.0	10.6
	WACCM-Hist	0.78	6.7	2.7	11.2
	T0	0.51	7.9	2.1	15.0
	T1	0.57	6.7	1.2	13.1
Europe	CAM-chem-SD	0.91	3.7	1.4	6.0
	WACCM-SD	0.90	3.8	1.3	6.4
	WACCM-AMIP	0.92	3.8	3.1	4.4
	WACCM-Hist	0.91	4.0	3.3	4.7
	T0	0.92	3.1	1.1	4.8
	T1	0.92	2.8	0.5	4.0
Japan	CAM-chem-SD	0.84	7.7	4.3	13.3
	WACCM-SD	0.76	9.3	5.0	15.8
	WACCM-AMIP	0.64	8.9	6.3	14.2
	WACCM-Hist	0.63	9.6	6.1	15.7
	T0	0.73	10.8	6.9	17.8
	T1	0.79	9.5	5.8	15.7
Australia and New Zealand	CAM-chem-SD	0.93	4.0	5.8	2.0
	WACCM-SD	0.83	4.6	6.1	2.7
	WACCM-AMIP	0.79	3.7	4.9	2.1
	WACCM-Hist	0.79	3.7	5.0	2.1
	T0	0.98	3.5	5.1	1.8
	T1	0.97	3.7	5.3	1.9

Note. T0 and T1 comparisons are for only 2013, WACCM for 1990–2014, CAM-chem-SD for 2000–2014.
Abbreviations: JFM, January–February-March; JJA, June-July-August.

levels, grouped by latitude ranges. The comparisons show generally good agreement for all the simulations to the observations. The fractional mean difference is within 25% for most regions in the troposphere. One exception is the surface high latitudes comparison, where the model overestimates the measurements. This discrepancy is likely due to the lack of short-lived halogen chemistry in this version of the models which depletes surface springtime ozone at high latitudes (Fernandez et al., 2019). These results are very similar to the evaluation of the CAM-chem simulations for CCMI (Tilmes et al., 2016), and the standard CAM4-chem and CAM5-chem simulations (Tilmes et al., 2015). In a few cases, the seasonal variation (correlation) is rather poor at the surface (equatorial Americas and Japan), though the overall bias is very small.

5.2.3. Carbon Monoxide Evaluation

In this section we compare CESM2 to in situ measurements of carbon monoxide (CO) at surface sites and to retrievals of CO from satellite observations. CO has an atmospheric lifetime of 2–4 weeks, depending on season, with its primary loss due to reaction with the hydroxyl radical (OH). Calibrated CO dry air mixing ratio from weekly surface air samples collected around the world by the NOAA Global Monitoring Division Carbon Cycle Cooperative Global Air Sampling Network are available between 1988 and present (Petron et al., 2018). The mean CO averaged over 2010–2014 for each of the sample sites is shown in Figure 7a, illustrating the spatial coverage of the sampling as well as the large difference in Northern and Southern Hemisphere mixing ratios. Figure 7b shows the mean bias over 2010–2014 between several CESM2 simulations (CAM-chem-SD, WACCM-SD, and WACCM-AMIP) and the observations as a function of latitude. The model simulations underestimate the observations by ~40% over most of the Northern Hemisphere but less than ~10% in the Southern Hemisphere. At all latitudes the model captures, the seasonal variation fairly well, as shown by the large correlation coefficients (symbol size). The time series for several remote sites are shown in Figures 7c–7h, along with the CESM2 results, and the model bias. The model results are very similar for the three configurations and reproduce the seasonal cycle well at all of these locations. At high northern latitudes (panels c and d), there is a decreasing trend in the CO observations (Worden et al., 2013) that is not reproduced well in the simulations. In the tropics, CESM2 still underestimates the observations, but with a smaller bias (10–30%). In the southern midlatitudes (New Zealand), there is near-zero bias; however, at the South Pole, the site most remote from sources, the model slightly underestimates the observations by a few ppb.

Figure 8 shows comparisons for several regions between the CAM-chem-SD simulation and the time series (2001–2017) of CO retrieved from the Measurements of Pollution in The Troposphere (MOPITT) instrument onboard the Terra satellite (Drummond et al., 2010). The MOPITT V8 Joint (NIR + TIR) retrievals (Deeter et al., 2019) are used, which, over land, have a strong sensitivity to surface concentrations. The model is matched to the gridded monthly MOPITT observations, and the averaging kernel for each grid is applied to the model before regional averages are computed. The regions selected include those dominated by anthropogenic emissions (United States, Europe, and northern Asia), as well as regions strongly influenced by biomass burning (Southeast Asia, South America, Africa, and Australia). The model has a large negative bias in all the regions of the Northern Hemisphere, similar to the comparisons to the surface flask data shown above (in Figure 7). In contrast, in the Southern Hemisphere, the column average amounts and the seasonal variation, driven largely by biomass burning, are captured well by the model. The simulations of CO, and thus the model biases, are similar for all model configurations (not shown in Figure 8 for clarity), as seen in Figure 7, which is expected as they all use the same emissions inventory. The model bias for CO is very similar to that seen in previous versions of CESM with different emissions inventories, such as the CCMI simulations with CAM4-chem (Tilmes et al., 2016). The Northern Hemisphere underestimation of CO by the models is most likely due to missing anthropogenic emissions from the inventories used to drive the model, as seen in past model comparisons (e.g., Gaubert et al., 2017).

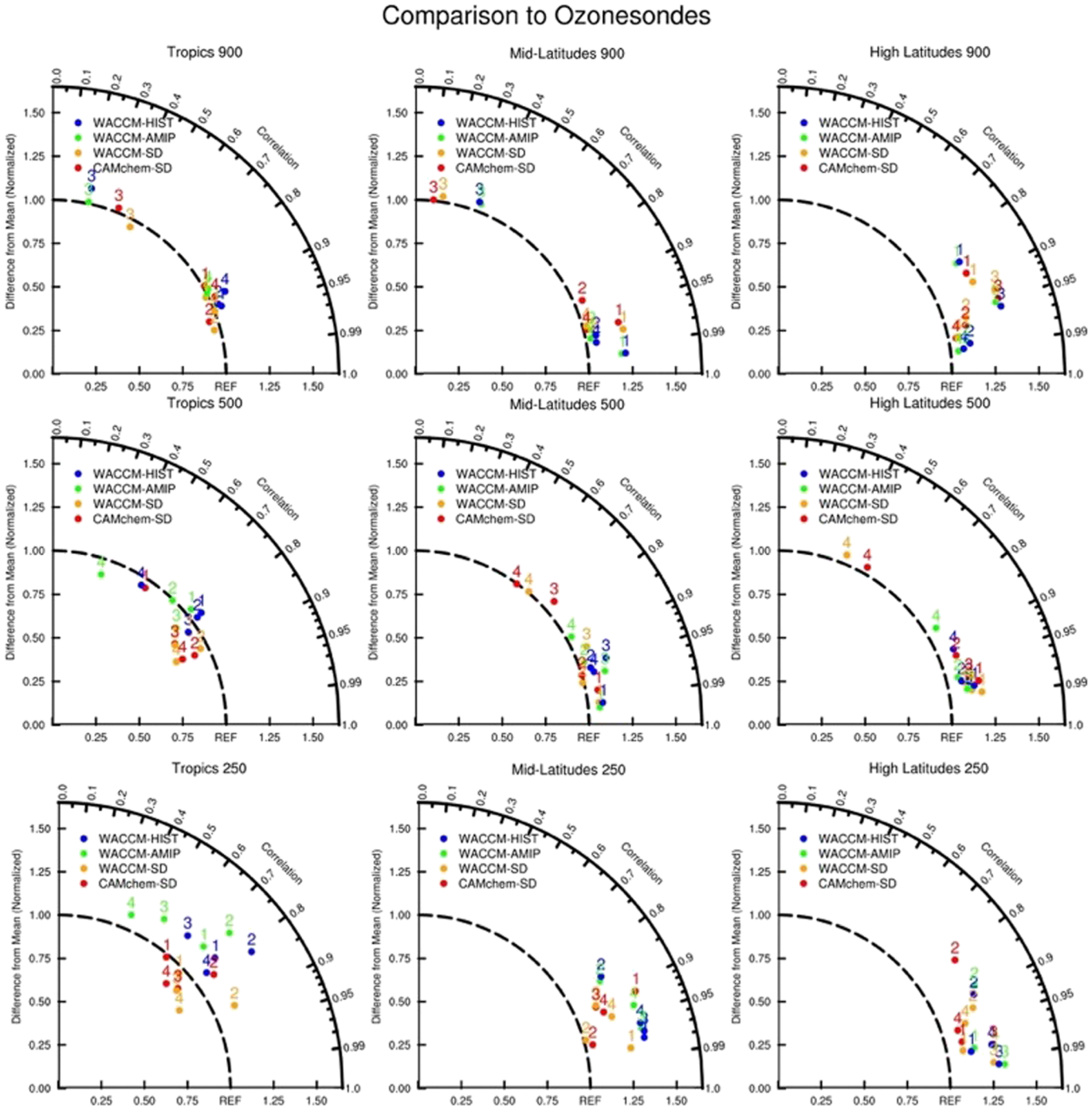

Figure 6. Taylor-like diagrams of the comparison of CESM2 simulations to a present-day (1995–2010) ozonesonde climatology (blue: WACCM-hist; green: WACCM-AMIP; orange: WACCM-SD; red: CAM-chem-SD). The normalized mean difference between simulations and observations for each region (number) is shown on the radius, and the correlation of the seasonal cycle is shown as the angle from the *y*-axis. Model results are interpolated to the locations of the observations (top: 900 hPa; middle: 500 hPa; bottom: 250 hPa). The numbers correspond to specific regions, as defined in Tilmes et al. (2012): Left panels (tropics): 1, NH subtropics; 2, W Pacific/E Indian Ocean; 3, Equatorial Americas; 4, Atlantic/Africa. Middle panels (midlatitudes): 1, Western Europe; 2, Eastern United States; 3, Japan; 4, SH midlatitudes. Right panels (high latitudes): 1, NH Polar West; 2. NH Polar East; 3, Canada; 4, SH polar.

5.2.4. Ethane and Propane Evaluation

Ethane (C_2H_6) is the most abundant nonmethane hydrocarbon (NMHC) in the remote troposphere and fairly well mixed due to its relatively long lifetime of 2 months (Simpson et al., 2012). Its sources are

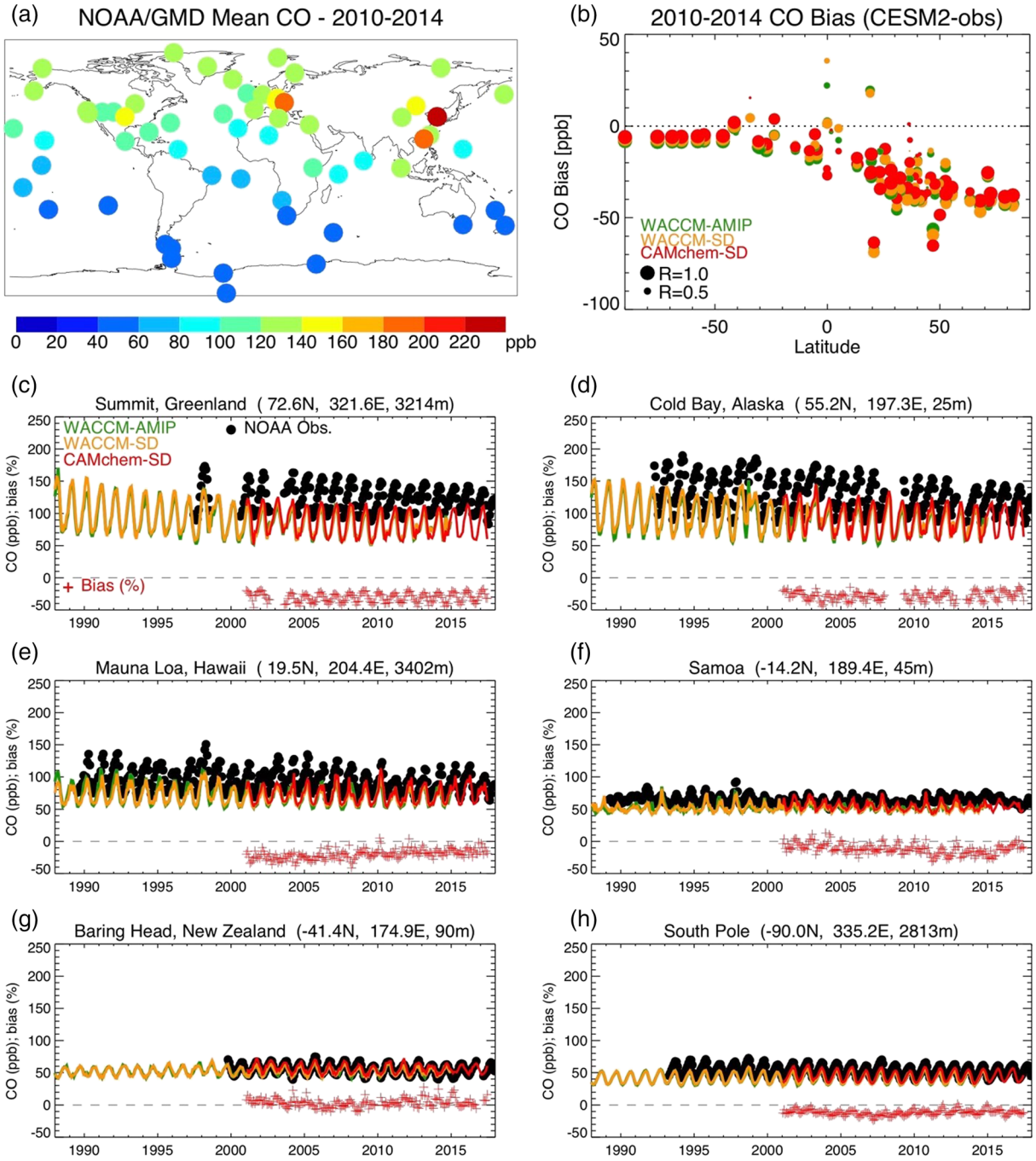

Figure 7. (a) Map of observed mean CO for 2000–2014 from NOAA/GMD flask samples. (b) Mean biases for 2000–2014 between CESM2 simulations and NOAA observations. (c–h) Comparison of CAM-chem-SD, WACCM-SD and WACCM-AMIP to NOAA/GMD surface CO measurements for time series at several remote sites: monthly mean CO and the fractional bias between each model simulation and observations.

primarily evaporative emissions from extraction and processing of fossil fuels, along with biofuel combustion and biomass burning (see Figure S1). Propane (C_3H_8) has primarily anthropogenic sources, such as liquefied petroleum gas, with a small contribution from biomass burning and ocean emissions (see Figure S1). Due to a faster reaction rate with OH, the abundance of propane in the remote atmosphere is significantly less than ethane.

Flask samples of ambient air collected since 1995 at coastal sites of the South and North Pacific Ocean, from New Zealand to Alaska, and analyzed for ethane and propane concentrations, provide a valuable data set for

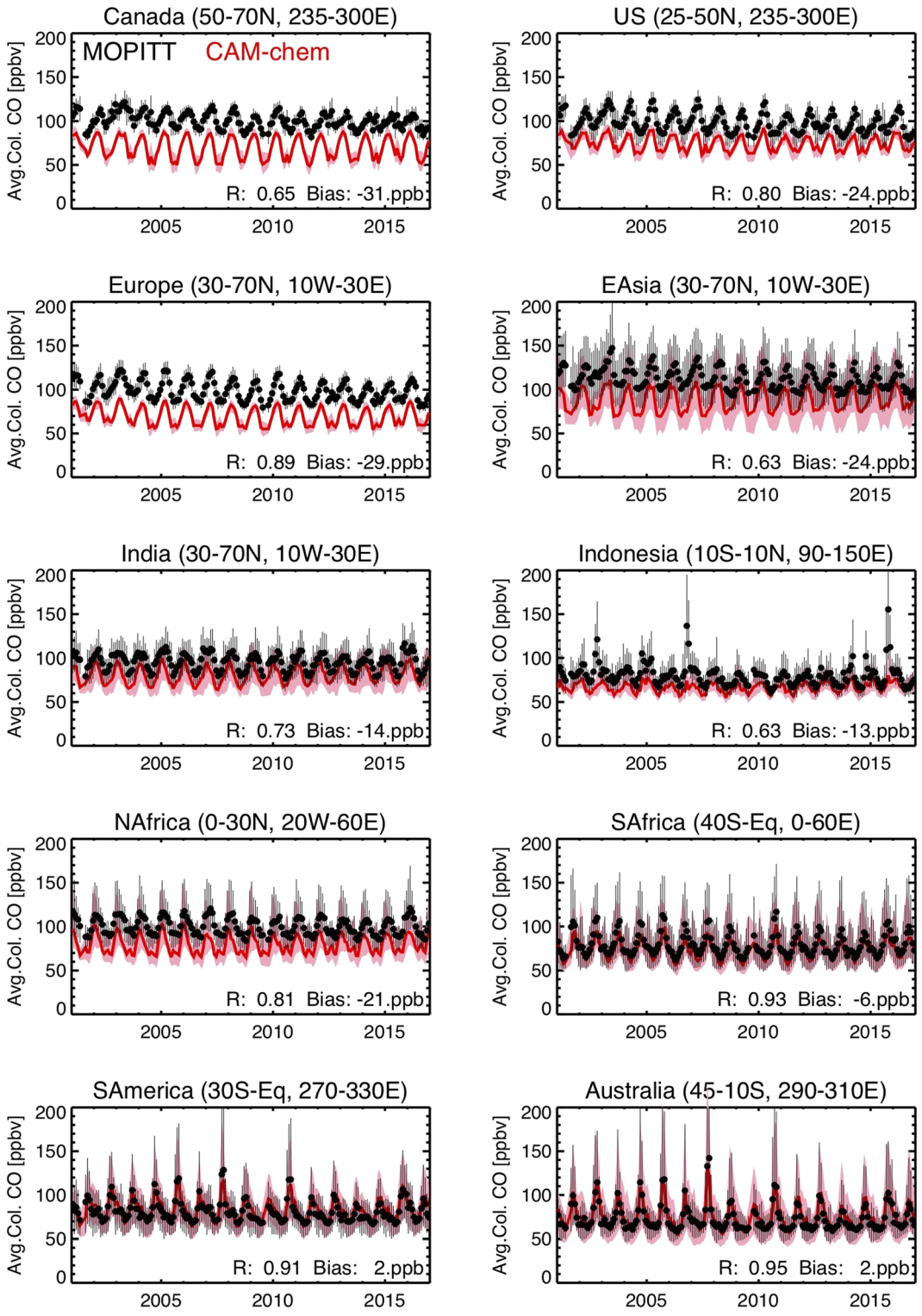

Figure 8. Time series evaluation of average column CO from CAM-chem-SD (red line) for various regions with MOPITT (black points). Red line is the mean, and pink shading indicates the range (minimum to maximum) of the model CO column for the region; black error bars show the range of MOPITT CO columns in the region.

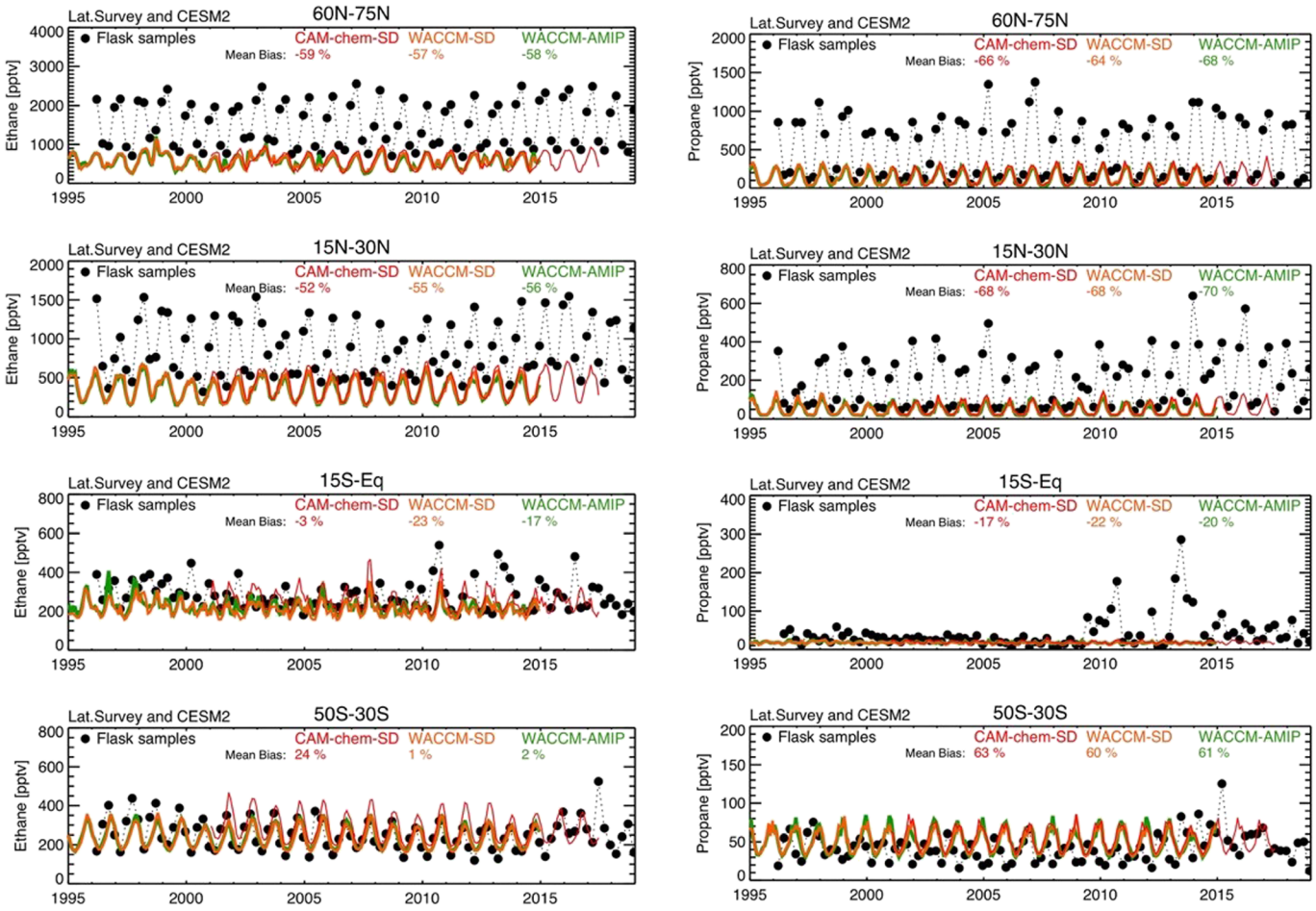

Figure 9. CESM2 evaluation of surface ethane (left panels) and propane (right panels) with flask measurements at coastal sites around the Pacific Ocean, averaged for four latitude bands (top to bottom: 60–75°N, 15–30°N, 15°S–equator, 50–30°S).

model evaluation (Blake, 2005; Simpson et al., 2012). The latitudinal survey observations are made four times each year, providing 60–80 samples in each season. Results from the CESM2 simulations at the surface along longitude 190°E are compared with these observations for four latitude bins in Figure 9. The CESM2 simulations grossly underestimate both ethane and propane mixing ratios in the NH for the years shown (>50% mean negative bias) but generally fall within the range of observations in the SH. Analyses of the observations show a long-term decreasing ethane trend from 1985 to about 2000 (Simpson et al., 2012), and a subsequent increase since the mid-2000s (Helmig et al., 2016), which appears in the anthropogenic emissions used to drive these simulations (Figure S1) but is difficult to discern in the modeled mixing ratios (Figure 9).

5.2.5. Evaluation With Aircraft Observations

Observations from airborne field experiments provide simultaneous measurements of numerous compounds, which allow for a comprehensive evaluation of model simulations of tropospheric composition. While each campaign provides data over limited spatial regions and short time periods, representative profiles from each campaign have been compiled to allow model evaluation over a wide range of locations and all seasons (Emmons et al., 2000; Tilmes et al., 2015). These "data composites" (not really a climatology as the observations are so sparse) are part of the standard CESM atmosphere diagnostics package (http://www.cesm.ucar.edu/working_groups/Atmosphere/amwg-diagnostics-package/). Results from the CESM2 simulations are shown with the observations in Figure 10. Each observation point represents an average over 2–7 km of the data composite profiles, and the model points are averages over the same location and altitude range for the corresponding month of the observation, averaged over years 1995–2010 for the WACCM-HIST and WACCM-AMIP simulations, and 2002–2010 for the SD cases.

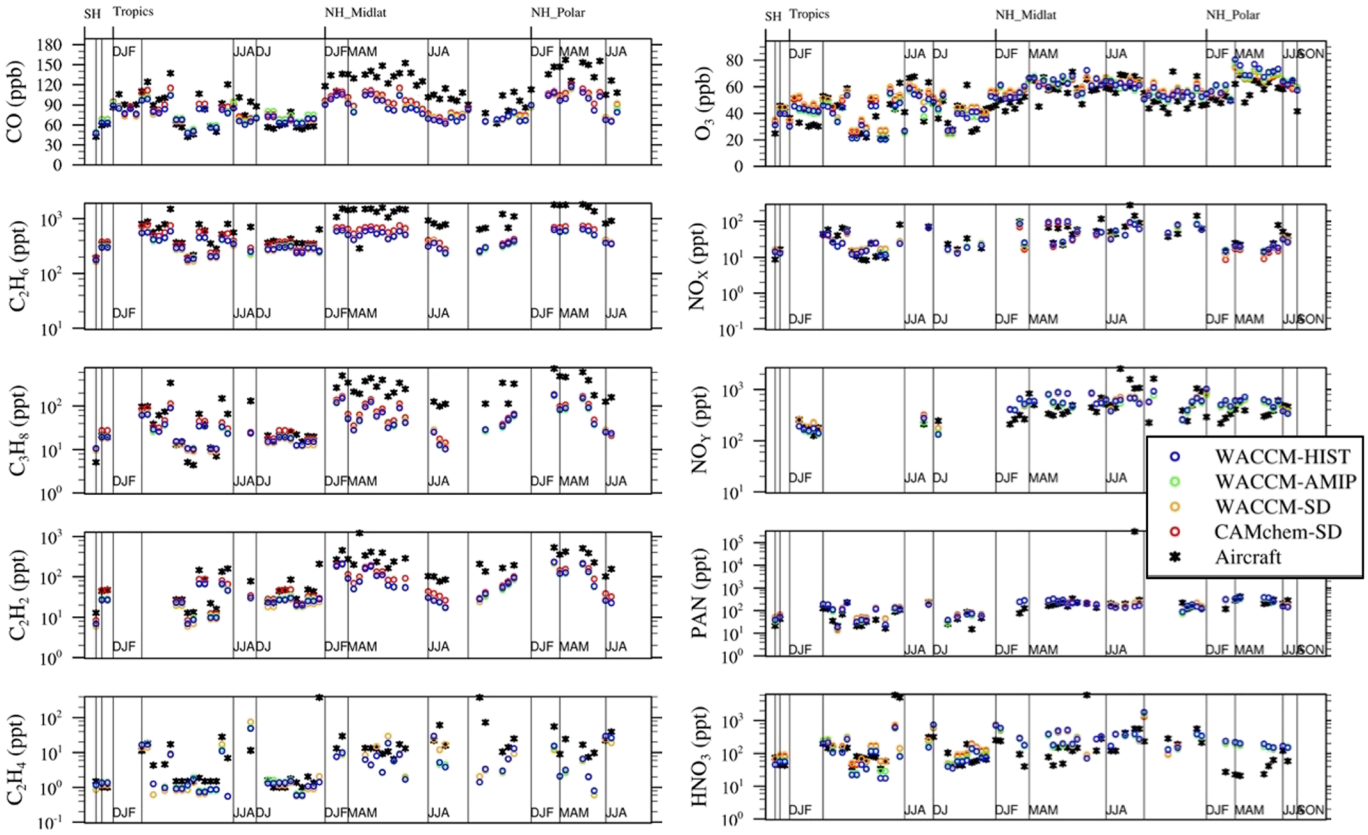

Figure 10. Evaluation of CESM2 simulations of tropospheric compounds with summaries of observations from aircraft campaigns, averaged over 2–7 km.

The model simulations are generally consistent for all of the species shown. The comparison for CO, ethane, and propane is similar to the evaluations presented above: the models agree with observations fairly well in the Southern Hemisphere and Tropics, but significantly underestimate them in northern midlatitude and high latitudes, particularly in winter and spring. The results are similar for a couple of other hydrocarbons not discussed before, C_2H_2 (ethyne) and C_2H_4 (ethene), that have primarily combustion sources, consistent with missing sources in the emissions inventories, as with CO. The comparison of ozone results is similar to that shown above in the ozonesonde evaluation. The model results show good agreement to both NO and PAN observations; however HNO_3, and consequently NO_y (which is the sum of NO_x, PAN, HNO_3 and other reactive nitrogen compounds), is overestimated by the model in some locations. Since HNO_3 is highly soluble, this could be an indication of the model not simulating sufficient washout on those occasions.

6. Discussion and Conclusions

The updated tropospheric MOZART chemical mechanism (T1) includes improved representation of the oxidation of isoprene, terpenes and aromatic compounds, particularly for reactive nitrogen reservoirs, thus improving the simulation of ozone distributions in the lower troposphere. The more detailed representation of organic nitrates in MOZART-T1 allows for tracing the interaction of anthropogenic pollutants and natural compounds and their impact on air quality as well as ecosystem health through deposition. Many of the new species included in the mechanism are now observed directly in the atmosphere, allowing for evaluation of the model chemistry in greater detail, as is shown in Schwantes et al. (2020).

A number of observational datasets provide long-term measurements of ozone, carbon monoxide, and hydrocarbons, allowing evaluation of the CESM2 simulations provided for CMIP6 covering the past couple of decades. The carbon monoxide, ethane, and propane distributions in CESM2 are significantly underestimated in the Northern Hemisphere, most likely due to the underestimate of the anthropogenic emissions inventory provided for use in CMIP6, similar to previous inventories. Although not frequently used in

chemistry-climate model evaluations, observations of hydrocarbons are valuable for model evaluation to identify errors in ozone precursors and thus errors in the ozone production rates. The long-term surveys provided from flask samples collected the length of the Pacific Ocean are one such observational data set and indicate a significant underestimation in the Northern Hemisphere emissions of ethane and propane and likely other hydrocarbons. The ethane emissions used in CESM2 are about 11 Tg/year (based on Hoesly et al., 2018), which is lower than previous inverse modeling analyses that derived ~13 Tg/year (Xiao et al., 2008), 12.5 Tg/year (Pozzer et al., 2010), and ~15 Tg/year (Monks et al., 2018). The study by Monks et al. (2018) also illustrated that increasing the ethane emissions to match observations resulted in increases in acetaldehyde, PAN, and ozone. Propane is also an important ozone precursor. Thus, the CESM2 underestimation of hydrocarbons (based on the CMIP6 emissions), such as ethane and propane, likely lead to an underestimate of other tropospheric constituents, as will other models using the CMIP6 emissions. An on-going effort by the community to compile more accurate emissions inventories is needed to accurately simulate the sensitivity of ozone production to changes in its precursors.

Comparisons to ozonesonde observations throughout the troposphere show good agreement and some improvements over previous versions. While CESM2 shows a high bias for surface ozone in some regions, the seasonal cycle is reproduced well. Further improvement of the simulation of surface ozone will require simultaneous improvement of the emissions of ozone precursors (i.e, CO, hydrocarbons, and NO_x), the chemical mechanism for the oxidation of VOCs and NO_x, and the representation of physical influences on ozone, such as dry deposition to land and ocean surfaces (e.g., Clifton et al., 2019). An expansion of the terpene oxidation chemistry has been developed (MOZART-T2), which further improves the simulation of surface ozone particularly in forested regions (Schwantes et al., 2020). That work presents a detailed evaluation of the T1 and T2 mechanisms for the southeastern United States showing that the increased chemical complexity of T2 allows for reproduction of many observed oxidation products, as well as improving the simulation of surface ozone.

This paper is intended to serve as a reference for the chemistry in CESM2 (Danabasoglu et al., 2020), including for the WACCM6 simulations submitted to CMIP6 (Gettelman et al., 2019), and companion paper to the presentation of the SOA simulation results (Tilmes et al., 2019). The chemistry mechanisms for CAM-chem and WACCM configurations of CESM have been updated for CESM2 over previous versions, particularly for tropospheric chemistry. CESM provides flexibility in the chemical mechanism used in simulations, which can be readily modified by users. Future releases of CESM will include options for additional chemical mechanisms, such as a more comprehensive representation of terpene chemistry (Schwantes et al., 2020). A detailed mechanism of very short lived halogens has also been developed for CESM (Fernandez et al., 2019) and will be released in a future version. Development of mechanisms that are less computationally costly is also underway. Through participation in model intercomparison activities, as well as focused studies and analyses of field campaign observations, the chemistry components of CESM will continue to evolve as areas of needed improvement are identified.

Acknowledgments
The CESM project is supported primarily by the National Science Foundation (NSF). We thank all the scientists and software engineers who contributed to the development of CESM2. This material is based upon work supported by the National Center for Atmospheric Research, which is a major facility sponsored by the NSF under Cooperative Agreement No. 1852977. Computing and data storage resources, including the Cheyenne supercomputer (doi:https://10.5065/D6RX99HX), were provided by the Computational and Information Systems Laboratory (CISL) at NCAR. We acknowledge the TOAR initiative (http://www.igacproject.org/activities/TOAR) for providing the TOAR surface ozone database (https://doi.org/10.1594/PANGAEA.876108). The retrievals of carbon monoxide from the Terra/MOPITT (Measurements Of Pollution in The Troposphere) instrument are available from the NASA Earthdata archive (https://earthdata.nasa.gov; ftp://l5ftl01.larc.nasa.gov/MOPITT/). The surface observations of carbon monoxide are freely available from the NOAA Earth System Research Laboratory Global Monitoring Division data archive (https://www.esrl.noaa.gov/gmd/dv/ftpdata.html). The surface flask sampling observations of ethane and propane from the University of California at Irvine are available at the ESS-DIVE archive (https://data.ess-dive.lbl.gov/view/doi:10.3334/CDIAC/ATG.002). All CESM2 simulations presented here are freely available through the Climate Data Gateway (https://www.earthsystemgrid.org/). The CAM-chem-SD simulations are available at: https://www2.acom.ucar.edu/gcm/cam-chem-output (https://doi.org/10.5065/NMP7-EP60). We thank Gabriele Pfister, Gustavo Cuchiara, Siyuan Wang, and two anonymous reviewers for their helpful comments that improved this manuscript.

References

Andres, R., & Kasgnoc, A. (1998). A time-averaged inventory of subaerial volcanic sulfur emissions. *Journal of Geophysical Research-Atmospheres*, *103*(D19), 25,251–25,261. https://doi.org/10.1029/98JD02091

Blake, D. (2005). Methane, Nonmethane Hydrocarbons, Alkyl Nitrates, and Chlorinated Carbon Compounds including 3 Chlorofluorocarbons (CFC-11, CFC-12, and CFC-113) in Whole-air Samples (April 1979–December 2012). In *Carbon Dioxide Information Analysis Center (CDIAC)*. Oak Ridge, TN (United States): Oak Ridge National Laboratory (ORNL). https://doi.org/10.3334/CDIAC/ATG.002

Bloss, C., Wagner, V., Jenkin, M. E., Volkamer, R., Bloss, W. J., Lee, J. D., et al. (2005). Development of a detailed chemical mechanism (MCMv3.1) for the atmospheric oxidation of aromatic hydrocarbons. *Atmospheric Chemistry and Physics*, *5*(3), 641–664. https://doi.org/10.5194/acp-5-641-2005

Bouvier-Brown, N., Goldstein, A., Worton, D., Matross, D., Gilman, J., Kuster, W., et al. (2009). Methyl chavicol: Characterization of its biogenic emission rate, abundance, and oxidation products in the atmosphere. *Atmospheric Chemistry and Physics*, *9*(6), 2061–2074. https://doi.org/10.5194/acp-9-2061-2009

Brasseur, G., Hauglustaine, D., Walters, S., Rasch, P., Muller, J., Granier, C., & Tie, X. (1998). MOZART, a global chemical transport model for ozone and related chemical tracers 1. Model description. *Journal of Geophysical Research-Atmospheres*, *103*(D21), 28,265–28,289. https://doi.org/10.1029/98JD02397

Buchholz, R. R., Emmons, L. K., Tilmes, S., & the CESM2 development team (2019). CESM2.1/CAM-chem instantaneous output for boundary conditions. UCAR/NCAR - Atmospheric Chemistry Observations and Modeling Laboratory. Accessed 1 June 2019, https://doi.org/10.5065/NMP7-EP60

Burkholder, J. B., Sander, S. P., Abbatt, J., Barker, J. R., Huie, R. E., Kolb, C. E., et al. (2015). Chemical kinetics and photochemical data for use in atmospheric studies, evaluation no. 18, JPL Publication 15–10, Jet Propulsion Laboratory, Pasadena, CA. Retrieved from http://jpldataeval.jpl.nasa.gov

Calvert, J. G., Atkinson, R., Becker, K. H., Kamens, R. M., Seinfeld, J. H., Wallington, T. J., & Yarwood, G. (2002). *The mechanisms of atmospheric oxidation of aromatic hydrocarbons*. New York: Oxford University Press.

Carlton, A., de Gouw, J., Jimenez, J. L., Ambrose, J. L., Brown, S., Baker, K. R., et al. (2018). Synthesis of the southeast atmosphere studies: Investigating fundamental atmospheric chemistry questions. *Bulletin of the American Meteorological Society*, *99*(3), 547–567. https://doi.org/10.1175/BAMS-D-16-0048.1

Clifton, O. E., Fiore, A. M., Munger, J. W., & Wehr, R. (2019). Spatiotemporal controls on observed daytime ozone deposition velocity over northeastern U.S. forests during summer. *Journal of Geophysical Research: Atmospheres*, *124*, 5612–5628. https://doi.org/10.1029/2018JD029073

Danabasoglu, G. (2019a). NCAR CESM2-WACCM model output prepared for CMIP6 CMIP amip. Version 20191105. *Earth System Grid Federation*. https://doi.org/10.22033/ESGF/CMIP6.10041

Danabasoglu, G. (2019b). NCAR CESM2-WACCM model output prepared for CMIP6 CMIP historical. Version 20191105. *Earth System Grid Federation*. https://doi.org/10.22033/ESGF/CMIP6.10071

Danabasoglu, G., Lamarque, J. F., Bacmeister, J., Bailey, D. A., DuVivier, A. K., Edwards, J., et al. (2020). The Community Earth System Model version 2 (CESM2). *Journal of Advances in Modeling Earth Systems*, *12*, e2019MS001916. https://doi.org/10.1029/2019MS001916

Darmenov, A. S. and da Silva, A.: The Quick Fire Emissions Dataset (QFED): Documentation of versions 2.1, 2.2 and 2.4, in: Technical Report Series on Global Modeling and Data Assimilation, edited by: Koster, R. D., 212 pp., NASA Goddard Space Flight Center, Greenbelt, MD, USA, 2015.

Deeter, M. N., Edwards, D. P., Francis, G. L., Gille, J. C., Mao, D., Martínez-Alonso, S., et al. (2019). Radiance-based retrieval bias mitigation for the MOPITT instrument: the version 8 product. *Atmospheric Measurement Techniques*, *12*(8), 4561–4580. https://doi.org/10.5194/amt-12-4561-2019

Drummond, J., Zou, J., Nichitiu, F., Kar, J., Deschambaut, R., & Hackett, J. (2010). A review of 9-year performance and operation of the MOPITT instrument. *Advances in Space Research*, *45*(6), 760–774. https://doi.org/10.1016/j.asr.2009.11.019

Emmons, L. K., Hauglustaine, D. A., Müller, J. F., Carroll, M. A., Brasseur, G. P., Brunner, D., et al. (2000). Data composites of airborne observations of tropospheric ozone and its precursors. *Journal of Geophysical Research-Atmospheres*, *105*(D16), 20497–20538. https://doi.org/10.1029/2000jd900232

Emmons, L. K., Walters, S., Hess, P. G., Lamarque, J. F., Pfister, G. G., Fillmore, D., et al. (2010). Description and evaluation of the Model for Ozone and Related chemical Tracers, version 4 (MOZART-4). *Geoscientific Model Development*, *3*(1), 43–67. https://doi.org/10.5194/gmd-3-43-2010

Eyring, V., Bony, S., Meehl, G., Senior, C., Stevens, B., Stouffer, R., & Taylor, K. (2016). Overview of the Coupled Model Intercomparison Project Phase 6 (CMIP6) experimental design and organization. *Geoscientific Model Development*, *9*(5), 1937–1958. https://doi.org/10.5194/gmd-9-1937-2016

Fernandez, R. P., Carmona-Balea, A., Cuevas, C. A., Barrera, J. A., Kinnison, D. E., Lamarque, J.-F., et al. (2019). Modeling the sources and chemistry of polar tropospheric halogens (Cl, Br, and I) using the CAM-Chem global chemistry-climate model. *Journal of Advances in Modeling Earth Systems*, *11*(7), 2259–2289. https://doi.org/10.1029/2019MS001655

Fisher, J., Jacob, D., Travis, K., Kim, P., Marais, E., Miller, C., et al. (2016). Organic nitrate chemistry and its implications for nitrogen budgets in an isoprene- and monoterpene-rich atmosphere: Constraints from aircraft (SEAC(4)RS) and ground-based (SOAS) observations in the southeast US. *Atmospheric Chemistry and Physics*, *16*(9), 5969–5991. https://doi.org/10.5194/acp-16-5969-2016

Gaubert, B., Worden, H. M., Arellano, A. F. J., Emmons, L. K., Tilmes, S., Barré, J., et al. (2017). Chemical feedback from decreasing carbon monoxide emissions. *Geophysical Research Letters*, *44*(19), 9985–9995. https://doi.org/10.1002/2017gl074987

Gettelman, A., Mills, M. J., Kinnison, D. E., Garcia, R. R., Smith, A. K., Marsh, D. R., et al. (2019). The Whole Atmosphere Community Climate Model Version 6 (WACCM6). *Journal of Geophysical Research: Atmospheres*, *124*(23), 12,380–12,403. https://doi.org/10.1029/2019JD030943

Granier, C., J.F. Lamarque, A. Mieville, J.F. Muller, J. Olivier, J. Orlando, et al., POET, a database of surface emissions of ozone precursors, (http://accent.aero.jussieu.fr/Documents/POET_documentation.pdf, available at https://eccad3.sedoo.fr/), 2005.

Guenther, A. B., Jiang, X., Heald, C. L., Sakulyanontvittaya, T., Duhl, T., Emmons, L. K., & Wang, X. (2012). The Model of Emissions of Gases and Aerosols from Nature version 2.1 (MEGAN2.1): An extended and updated framework for modeling biogenic emissions. *Geoscientific Model Development*, *5*(6), 1471–1492. https://doi.org/10.5194/gmd-5-1471-2012

He, J., Zhang, Y., Tilmes, S., Emmons, L., Lamarque, J. F., Glotfelty, T., et al. (2015). CESM/CAM5 improvement and application: Comparison and evaluation of updated CB05_GE and MOZART-4 gas-phase mechanisms and associated impacts on global air quality and climate. *Geoscientific Model Development*, *8*(12), 3999–4025. https://doi.org/10.5194/gmd-8-3999-2015

Helmig, D., Rossabi, S., Hueber, J., Tans, P., Montzka, S. A., Masarie, K., et al. (2016). Reversal of global atmospheric ethane and propane trends largely due to US oil and natural gas production. *Nature Geoscience*, *9*(7), 490–495. https://doi.org/10.1038/ngeo2721

Hoesly, R., Smith, S., Feng, L., Klimont, Z., Janssens-Maenhout, G., Pitkanen, T., et al. (2017). Historical Emissions (1750 - 2014) - CEDS - v2017-05-18. Version 20170519. *Earth System Grid Federation*. https://doi.org/10.22033/ESGF/input4MIPs.1241

Hoesly, R. M., Smith, S. J., Feng, L., Klimont, Z., Janssens-Maenhout, G., Pitkanen, T., et al. (2018). Historical (1750-2014) anthropogenic emissions of reactive gases and aerosols from the Community Emissions Data System (CEDS). *Geoscientific Model Development*, *11*(1), 369–408. https://doi.org/10.5194/gmd-11-369-2018

Horowitz, L. W., Walters, S., Mauzerall, D. L., Emmons, L. K., Rasch, P. J., Granier, C., et al. (2003). A global simulation of tropospheric ozone and related tracers: Description and evaluation of MOZART, version 2. *Journal of Geophysical Research-Atmospheres*, *108*(D24), 4784. https://doi.org/10.1029/2002jd002853

Kinnison, D. E., Brasseur, G. P., Walters, S., Garcia, R. R., Marsh, D. R., Sassi, F., et al. (2007). Sensitivity of chemical tracers to meteorological parameters in the MOZART-3 chemical transport model. *Journal of Geophysical Research-Atmospheres*, *112*(D20), D20302. https://doi.org/10.1029/2006jd007879

Knote, C., Hodzic, A., Jimenez, J. L., Volkamer, R., Orlando, J. J., Baidar, S., et al. (2014). Simulation of semi-explicit mechanisms of SOA formation from glyoxal in aerosol in a 3-D model. *Atmospheric Chemistry and Physics*, *14*(12), 6213–6239. https://doi.org/10.5194/acp-14-6213-2014

Lamarque, J. F., Emmons, L. K., Hess, P. G., Kinnison, D. E., Tilmes, S., Vitt, F., et al. (2012). CAM-chem: Description and evaluation of interactive atmospheric chemistry in the Community Earth System Model. *Geoscientific Model Development*, *5*(2), 369–411. https://doi.org/10.5194/gmd-5-369-2012

Liu, X., Ma, P. L., Wang, H., Tilmes, S., Singh, B., Easter, R. C., et al. (2016). Description and evaluation of a new four-mode version of the Modal Aerosol Module (MAM4) within version 5.3 of the Community Atmosphere Model. *Geoscientific Model Development*, *9*(2), 505–522. https://doi.org/10.5194/gmd-9-505-2016

Mahowald, N., Lamarque, J., Tie, X., & Wolff, E. (2006). Sea-salt aerosol response to climate change: Last Glacial Maximum, preindustrial, and doubled carbon dioxide climates. *Journal of Geophysical Research-Atmospheres*, *111*(D5). https://doi.org/10.1029/2005JD006459

Mahowald, N., Muhs, D., Levis, S., Rasch, P., Yoshioka, M., Zender, C., & Luo, C. (2006). Change in atmospheric mineral aerosols in response to climate: Last glacial period, preindustrial, modern, and doubled carbon dioxide climates. *Journal of Geophysical Research-Atmospheres*, *111*(D10). https://doi.org/10.1029/2005JD006653

Marsh, D., Garcia, R., Kinnison, D., Boville, B., Sassi, F., Solomon, S., & Matthes, K. (2007). Modeling the whole atmosphere response to solar cycle changes in radiative and geomagnetic forcing. *Journal of Geophysical Research-Atmospheres*, *112*(D23). https://doi.org/10.1029/2006JD008306

Meinshausen, M., Vogel, E., Nauels, A., Lorbacher, K., Meinshausen, N., Etheridge, D. M., et al. (2017). Historical greenhouse gas concentrations for climate modelling (CMIP6). *Geoscientific Model Development*, *10*(5), 2057–2116. https://doi.org/10.5194/gmd-10-2057-2017

Mills, M., Schmidt, A., Easter, R., Solomon, S., Kinnison, D., Ghan, S., et al. (2016). Global volcanic aerosol properties derived from emissions, 1990-2014, using CESM1(WACCM). *Journal of Geophysical Research-Atmospheres*, *121*(5), 2332–2348. https://doi.org/10.1002/2015JD024290

Molod, A., Takacs, L., Suarez, M., & Bacmeister, J. (2015). Development of the GEOS-5 atmospheric general circulation model: Evolution from MERRA to MERRA2. *Geoscientific Model Development*, *8*(5), 1339–1356. https://doi.org/10.5194/gmd-8-1339-2015

Monks, S., Wilson, C., Emmons, L., Hannigan, J., Helmig, D., Blake, N., & Blake, D. (2018). Using an inverse model to reconcile differences in simulated and observed global ethane concentrations and trends between 2008 and 2014. *Journal of Geophysical Research-Atmospheres*, *123*(19), 11,262–11,282. https://doi.org/10.1029/2017JD028112

Neely III, R.R.; Schmidt, A., VolcanEESM: Global volcanic sulphur dioxide (SO_2) emissions database from 1850 to present - Version 1.0. Centre for Environmental Data Analysis, doi:https://doi.org/10.5285/76ebdc0b-0eed-4f70-b89e-55e606bcd568, 2016.

Neu, J., & Prather, M. (2012). Toward a more physical representation of precipitation scavenging in global chemistry models: Cloud overlap and ice physics and their impact on tropospheric ozone. *Atmospheric Chemistry and Physics*, *12*(7), 3289–3310. https://doi.org/10.5194/acp-12-3289-2012

Orlando, J., & Tyndall, G. (2012). Laboratory studies of organic peroxy radical chemistry: An overview with emphasis on recent issues of atmospheric significance. *Chemical Society Reviews*, *41*(19), 6294–6317. https://doi.org/10.1039/c2cs35166h

Paulot, F., Crounse, J., Kjaergaard, H., Kroll, J., Seinfeld, J., & Wennberg, P. (2009). Isoprene photooxidation: New insights into the production of acids and organic nitrates. *Atmospheric Chemistry and Physics*, *9*(4), 1479–1501. https://doi.org/10.5194/acp-9-1479-2009

Paulot, F., Crounse, J., Kjaergaard, H., Kurten, A., St Clair, J., Seinfeld, J., & Wennberg, P. (2009). Unexpected epoxide formation in the gas-phase photooxidation of isoprene. *Science*, *325*(5941), 730–733. https://doi.org/10.1126/science.1172910

Peeters, J., Muller, J., Stavrakou, T., & Nguyen, V. (2014). Hydroxyl radical recycling in isoprene oxidation driven by hydrogen bonding and hydrogen Tunneling: The upgraded LIM1 mechanism. *Journal of Physical Chemistry A*, *118*(38), 8625–8643. https://doi.org/10.1021/jp5033146

Peeters, J., Nguyen, T., & Vereecken, L. (2009). HOx radical regeneration in the oxidation of isoprene. *Physical Chemistry Chemical Physics*, *11*(28), 5935–5939. https://doi.org/10.1039/b908511d

Petron, G., A.M. Crotwell, P.M. Lang, E. Dlugokencky, Atmospheric carbon monoxide dry air mole fractions from the NOAA ESRL carbon cycle cooperative global air sampling network, 1988–2017, Version: 2018-10-17, Path: ftp://aftp.cmdl.noaa.gov/data/trace_gases/co/flask/surface/ (accessed 17 Dec 2018), 2018.

Porter, W., Safieddine, S., & Heald, C. (2017). Impact of aromatics and monoterpenes on simulated tropospheric ozone and total OH reactivity. *Atmospheric Environment*, *169*, 250–257. https://doi.org/10.1016/j.atmosenv.2017.08.048

Pozzer, A., Pollmann, J., Taraborrelli, D., Jöckel, P., Helmig, D., Tans, P., et al. (2010). Observed and simulated global distribution and budget of atmospheric C-2-C-5 alkanes. *Atmospheric Chemistry and Physics*, *10*(9), 4403–4422. https://doi.org/10.5194/acp-10-4403-2010

Price, C., Penner, J., & Prather, M. (1997). NO_x from lightning: 1. Global distribution based on lightning physics. *Journal of Geophysical Research-Atmospheres*, *102*(D5), 5929–5941. https://doi.org/10.1029/96JD03504

Schultz, M. G., Schröder, S., Lyapina, O., Cooper, O., Galbally, I., Petropavlovskikh, I., et al. (2017). Tropospheric ozone assessment report: Database and metrics data of global surface ozone observations. *Elementa-Science of the Anthropocene*, *5*(0), 58. https://doi.org/10.1525/elementa.244

Schumann, U., & Huntrieser, H. (2007). The global lightning-induced nitrogen oxides source. *Atmospheric Chemistry and Physics*, *7*(14), 3823–3907. https://doi.org/10.5194/acp-7-3823-2007

Schwantes, R. H., Emmons, L. K., Orlando, J. J., Barth, M. C., Tyndall, G. S., Hall, S. R., et al. (2020). Comprehensive isoprene and terpene gas-phase chemistry improves simulated surface ozone in the southeastern US. *Atmospheric Chemistry and Physics*, *20*(6), 3739–3776. https://doi.org/10.5194/acp-20-3739-2020

Simpson, I., Andersen, M., Meinardi, S., Bruhwiler, L., Blake, N., Helmig, D., et al. (2012). Long-term decline of global atmospheric ethane concentrations and implications for methane. *Nature*, *488*(7412), 490–494. https://doi.org/10.1038/nature11342

Taylor, K. (2001). Summarizing multiple aspects of model performance in a single diagram. *Journal of Geophysical Research-Atmospheres*, *106*(D7), 7183–7192. https://doi.org/10.1029/2000JD900719

Tilmes, S., Hodzic, A., Emmons, L. K., Mills, M. J., Gettelman, A., Kinnison, D. E., et al. (2019). Climate forcing and trends of organic aerosols in the Community Earth System Model (CESM2). *J. Adv. Model. Earth Sys. (CESM2 special issue)*, *11*(12), 4323–4351. https://doi.org/10.1029/2019MS001827

Tilmes, S., Lamarque, J. F., Emmons, L. K., Conley, A., Schultz, M. G., Saunois, M., et al. (2012). Technical note: Ozonesonde climatology between 1995 and 2011: Description, evaluation and applications. *Atmospheric Chemistry and Physics*, *12*(16), 7475–7497. https://doi.org/10.5194/acp-12-7475-2012

Tilmes, S., Lamarque, J. F., Emmons, L. K., Kinnison, D. E., Ma, P. L., Liu, X., et al. (2015). Description and evaluation of tropospheric chemistry and aerosols in the Community Earth System Model (CESM1.2). *Geoscientific Model Development*, *8*(5), 1395–1426. https://doi.org/10.5194/gmd-8-1395-2015

Tilmes, S., Lamarque, J. F., Emmons, L. K., Kinnison, D. E., Marsh, D., Garcia, R. R., et al. (2016). Representation of the Community Earth System Model (CESM1) CAM4-chem within the Chemistry-Climate Model Initiative (CCMI). *Geoscientific Model Development*, *9*(5), 1853–1890. https://doi.org/10.5194/gmd-9-1853-2016

Toon, O., Maring, H., Dibb, J., Ferrare, R., Jacob, D., Jensen, E., et al. (2016). Planning, implementation, and scientific goals of the studies of emissions and atmospheric composition, clouds and climate coupling by regional surveys (SEAC(4)RS) field mission. *Journal of Geophysical Research-Atmospheres*, *121*(9), 4967–5009. https://doi.org/10.1002/2015JD024297

Travis, K. R., Jacob, D. J., Fisher, J. A., Kim, P. S., Marais, E. A., Zhu, L., et al. (2016). Why do models overestimate surface ozone in the Southeast United States? *Atmospheric Chemistry and Physics*, *16*(21), 13,561–13,577. https://doi.org/10.5194/acp-16-13561-2016

Val Martin, M., Heald, C., & Arnold, S. (2014). Coupling dry deposition to vegetation phenology in the Community Earth System Model: Implications for the simulation of surface O3. *Geophysical Research Letters*, *41*(8), 2988–2996. https://doi.org/10.1002/2014GL059651

van Marle, M., Kloster, S., Magi, B., Marlon, J., Daniau, A., Field, R., et al. (2017). Historic global biomass burning emissions for CMIP6 (BB4CMIP) based on merging satellite observations with proxies and fire models (1750-2015). *Geoscientific Model Development*, *10*(9), 3329–3357. https://doi.org/10.5194/gmd-10-3329-2017

van Marle, M. J. E., Kloster, S., Magi, B. I., Marlon, J. R., Daniau, A.-L., Field, R. D., et al. (2016). Biomass Burning emissions for CMIP6 (v1.2). Version 20161213. *Earth System Grid Federation*. https://doi.org/10.22033/ESGF/input4MIPs.1117

Wennberg, P., Bates, K., Crounse, J., Dodson, L., McVay, R., Mertens, L., et al. (2018). Gas-phase reactions of isoprene and its major oxidation products. *Chemical Reviews*, *118*(7), 3337–3390. https://doi.org/10.1021/acs.chemrev.7b00439

Worden, H., Deeter, M., Frankenberg, C., George, M., Nichitiu, F., Worden, J., et al. (2013). Decadal record of satellite carbon monoxide observations. *Atmospheric Chemistry and Physics*, *13*(2), 837–850. https://doi.org/10.5194/acp-13-837-2013

Xiao, Y., Logan, J., Jacob, D., Hudman, R., Yantosca, R., & Blake, D. (2008). Global budget of ethane and regional constraints on US sources. *Journal of Geophysical Research-Atmospheres*, *113*(D21). https://doi.org/10.1029/2007JD009415

Young, P. J., Naik, V., Fiore, A. M., Gaudel, A., Guo, J., Lin, M. Y., et al. (2018). Tropospheric Ozone Assessment Report: Assessment of global-scale model performance for global and regional ozone distributions, variability, and trends. *Elementa: Science of the Anthropocene*, *6*(1), 10. https://doi.org/10.1525/elementa.265